Dark matter and Dark Forces from a supersymmetric hidden sector

S. Andreas,[*] M. D. Goodsell,[†] A. Ringwald[‡]

Deutsches Elektronen-Synchrotron, DESY, Notkestraße 85, 22607 Hamburg, Germany

Abstract

We show that supersymmetric "Dark Force" models with gravity mediation are viable. To this end, we analyse a simple supersymmetric hidden sector model that interacts with the visible sector via kinetic mixing of a light Abelian gauge boson with the hypercharge. We include all induced interactions with the visible sector such as neutralino mass mixing and the Higgs portal term. We perform a detailed parameter space scan comparing the produced dark matter relic abundance and direct detection cross-sections to current experiments.

[*]sarah.andreas@desy.de

[†]mark.goodsell@desy.de

[‡]andreas.ringwald@desy.de

1 Introduction

There has been much interest recently in the possibility that there exists a hidden sector containing a dark matter particle coupled to a hidden U(1) gauge boson (a "Dark Force") having a mass of the order of a GeV that kinetically mixes with the photon [1–4]. Such a scenario could explain many astrophysical puzzles, such as the positron excess observed by PAMELA [5], ATIC [6], and Fermi [7], or the direct detection and annual modulation signal of DAMA [8], CoGeNT [9, 10] and CRESST [11] (if one ignores the disputed [12, 13] contradiction due to XENON 100 [14] and CDMS [15]). Following from the work of [16–18], elegantly simple supersymmetric models in the latter category were constructed in [19] and further examined in [20]. However, these works emphasized that, in order to obtain such a light hidden sector, supersymmetry breaking effects in the visible sector would necessarily be dominated by gauge mediation, in order that the masses should be acceptably small. Thus it is natural to ask whether confirmation of these observations would be in contradiction with gravity mediation; in other words, whether it is also possible to have a gravity-mediated spectrum of particles that can yield similar phenomenology. This is also linked to the interesting question as to whether these models can be embedded into string theory: such hidden sectors appear very naturally there - see e.g. [21–29] - but the problem of finding gauge mediation dominance over gravity mediation is notoriously difficult to achieve in globally consistent models.

Beyond the dark matter motivation it is also useful to ask what hidden sector models of this form coming from string theory are allowed or excluded by current observations. This is because, even if the hidden sector does not comprise (all) the dark matter, there are a wealth of experiments capable of probing Dark Forces over a very wide range of hidden gauge boson mass and kinetic mixing values. Kinetic mixing was considered in the context of the heterotic string in [24, 30–32]. It has been examined in type II strings in [21–23, 33–37]; in [23, 27] both masses and mixings were considered, and it was argued that the Dark Forces scenario could be accommodated provided that there is additional sequestering. In this work, we shall consider hidden sector models with the particle content and similar couplings to those in [19], but argue that when we have gravity mediation domination these can still give interesting phenomenological predictions under certain mild assumptions, without requiring additional sequestering relative to the visible sector. Although we will discuss the possible explanation of the signals found by DAMA and CoGeNT, these will therefore not be our primary motivation: rather we wish to explore how simple supersymmetric hidden dark sectors with a hidden U(1) can be constrained by observations.

The paper is organised as follows. In section 2 we describe the model of a supersymmetric dark sector that we shall be examining. This is followed by a summary of constraints upon hidden U(1)s with hidden matter charged under them in 3. There we also include the reach of future fixed target experiments, and illustrate these with an investigation of a simple toy model. Section 4 then contains the meat of the paper: the results of the parameter search over our supersymmetric dark sector model. We include additional technical details in the appendix: the hidden sector RGEs in appendix A; the spectrum of the model in appendix B (including the mass mixing matrix with the visible neutralino in B.2); a review of kinetic and mass mixing of a massive hidden gauge boson with the hypercharge and Z in appendix C; and a description of the Goldstone boson mixing in appendix D. In addition, in appendix E we discuss the supersymmetry-induced Higgs portal term and the mixing of the hidden and MSSM Higgs fields; we believe that although the existence of the term has been known in the literature the mixing terms have not been explicitly given elsewhere.

Included is a calculation of the induced coupling of the hidden dark matter Majorana fermion to nucleons.

2 Supersymmetric dark sectors

2.1 Supersymmetric kinetic mixing

We shall consider models that interact with the visible sector primarily through kinetic mixing of a hidden U(1) gauge field with the hypercharge. Hence we have a holomorphic kinetic mixing χ_h between hypercharge B_α with coupling g_Y (and gaugino the bino, b) and hidden gauge superfield X_α with coupling g_h (and gaugino written as λ) appearing in the Lagrangian density

$$\mathcal{L} \supset \int d^2\theta \left(\frac{1}{4g_Y^2} B^\alpha B_\alpha + \frac{1}{4g_h^2} X^\alpha X_\alpha - \frac{\chi_h}{2} B^\alpha X_\alpha \right). \tag{2.1}$$

The physical kinetic mixing in the canonical basis [23, 36] is then given by

$$\chi = g_Y g_h \text{Re}(\chi_h). \tag{2.2}$$

We shall assume no matter charged under both hidden and visible gauge groups so this relationship is valid at all energy scales. Since we are considering string-inspired models with a "hidden" U(1), that is, without matter charged under both the visible and hidden gauge groups, we shall take the value of the holomorphic kinetic mixing parameter to be of the order of a loop factor [23]:

$$\chi_h \equiv \frac{\kappa}{16\pi^2}. \tag{2.3}$$

Here κ is a number that must in principle be derived from the high-energy string model, but depends only logarithmically upon the spectrum thereof. We shall either take it to be equal to one, or to vary by at most an order of magnitude from unity [23, 26, 27]. We thus have

$$\chi = g_Y g_h \frac{\kappa}{16\pi^2}; \tag{2.4}$$

the most commonly taken value for χ is thus of the order of 10^{-3}, but smaller values correspond to decreasing the hidden gauge coupling which may be extremely small in the case of hyperweak groups [23, 27, 38]. Henceforth we shall always use the physical mixing χ.

As befits a well-studied subject, there are a variety of notations. In addition to using χ, we shall also adopt the notation used in [39]:

$$\chi \equiv -\sin\epsilon \equiv -s_\epsilon$$
$$\cos\epsilon \equiv c_\epsilon \equiv \sqrt{1-\chi^2}, \qquad \tan\epsilon \equiv t_\epsilon = -\frac{\chi}{\sqrt{1-\chi^2}}. \tag{2.5}$$

Note however that this differs to the expressions in [19], which defines $\chi = -\tilde{\epsilon} \equiv -t_{\tilde{\epsilon}}, s_{\tilde{\epsilon}} \equiv -\frac{\chi}{\sqrt{1-\chi^2}}, c_{\tilde{\epsilon}} \equiv \frac{1}{\sqrt{1-\chi^2}}$ although there they write ϵ instead of $\tilde{\epsilon}$ (we added the tilde to avoid confusion with the above). On the other hand, [40–45] defines $\delta \equiv -\chi$. However, a crucial novelty in this work is our relation (2.4) which we shall see in section 3.3 will lead to qualitatively different results for the cross-sections.

2.2 Hidden matter fields

The model that we shall consider is the simplest possible without adding dimensionful supersymmetric quantities. There are three chiral superfields S, H_+, H_- with H_+ and H_- charged under the hidden U(1) with charges ± 1. These appear in a superpotential with dimensionless coupling λ_S

$$W \supset \lambda_S S H_+ H_-. \tag{2.6}$$

This is inspired by D-brane models where the singlet is essentially the adjoint of the gauge group: the superpotential above arises due to the $N = 2$-like structure, and there is no renormalisable singlet potential due to this; alternatively, there may be $N = 2$ supersymmetry of the couplings at some scale, although we shall not enforce this. Such hidden sectors from string theory were considered in e.g. [25, 29], and the above model was studied with gauge mediation in [19] where it was termed a "hidden sector NMSSM," although we have set the cubic singlet term in the superpotential to zero. There then exists a global U(1) symmetry under which S and H_- are charged; string theory will not respect this, and we consider that it shall either be broken at higher order in the superpotential or through non-perturbative effects - but we shall assure that it will play no role in the following.

Once we include soft supersymmetry-breaking terms we have the approximate potential for the hidden sector

$$
\begin{aligned}
V =& |\lambda_S|^2 (|SH_+|^2 + |SH_-|^2 + |H_+H_-|^2) \\
&+ \frac{g_h^2}{2} (|H_+|^2 - |H_-|^2 - \xi)^2 \\
&+ m_+^2 |H_+|^2 + m_-^2 |H_-|^2 + m_S^2 |S|^2 \\
&+ (\lambda_S A_S S H_+ H_- + \frac{1}{2} M_\lambda \lambda \lambda + c.c.)
\end{aligned}
\tag{2.7}
$$

where $\xi = -\frac{\chi}{g_h} \xi_Y = \chi(g_Y/g_h) g_Y \frac{v^2}{4} \cos 2\beta$. The approximation lies in the D-term potential; the full form is found in appendix E.

A crucial difference for the phenomenology of the model once we consider gravity mediation is, however, that the gravitino is not the LSP, and therefore the dark matter can consist of stable hidden sector particles. We can thus perform a full analysis of the model, including the visible sector and its couplings, using micrOMEGAs [46–50] to determine the relic abundance and direct detection cross-sections.

2.3 Symmetry breaking through running

Just as in the MSSM the top Yukawa coupling can, through running from the GUT scale, induce electroweak symmetry breaking, so in the model we are considering the Yukawa coupling λ_S can induce breaking of the hidden gauge symmetry. By choosing the soft masses and couplings at the MSSM GUT scale we can then find models at the low energy scale with hidden gauge symmetry breaking. A priori the independent supersymmetric parameters are χ, g_h, λ_S and the soft masses $m_{H_\pm}, m_S, A_S$ and M_λ (the hidden gaugino mass) which we can choose at the high energy scale and run down.

Via (2.4) we are asserting a relation between χ and g_h. Thus if we take $\kappa = 1$ we reduce the number of free parameters in the model by one. However, as described above we shall in certain

plots allow an order of magnitude variation in κ; hence although this does not strictly reduce the number of parameters in the model, it does rather constrain them with important consequences. Finally we shall make one further assumption about the parameters: we shall take $m_{H_+} = m_{H_-}$ at the high energy scale. This is motivated by the fields $H_\pm$ being a non-chiral pair (note that we are taking no explicit Fayet-Iliopoulos term for the hidden $U(1)$ which would introduce a mass splitting). Otherwise we shall scan over the remaining parameters to find interesting models.

The two-loop RGEs for the model are given in appendix A. By taking $m_S > m_{H_\pm}$ at the high energy scale, the RGEs naturally drive the soft masses for $m_{H_\pm}^2$ to be negative at low energies, triggering hidden symmetry breaking.[1] The visible sector coupling via the kinetic mixing then determines which field (H_+ or H_-) condenses; without loss of generality we take χ to be negative and thus H_+ condenses. Defining $\Delta \equiv \sqrt{\lambda_S^2 \xi - m_+^2 \lambda_S^2 / g_h^2}$, we have the conditions for a stable minimum with $\langle H_+ \rangle = \Delta/\lambda_S$, all other expectation values zero:

$$
\begin{aligned}
0 &\leq \Delta^2 \\
0 &\leq m_-^2 + m_+^2 + m_S^2 + 2\Delta^2 \\
0 &\leq (m_-^2 + m_+^2 + \Delta^2)(m_S^2 + \Delta^2) - |A_S|^2 \Delta^2.
\end{aligned}
\tag{2.8}
$$

This is reviewed in appendix B. The hidden gauge boson mass is then given by

$$
m_{\gamma'} = (\sqrt{2} g_h / \lambda_S)\Delta.
\tag{2.9}
$$

We give two examples of the values obtained scanning over m_S and $\alpha_S \equiv \frac{\lambda_S^2}{4\pi}$ in figure 1.

2.4 Symmetry breaking induced by the visible sector

The mechanism for hidden gauge symmetry breaking promoted in work such as [19] is via the effective Fayet-Iliopoulos term induced in the hidden sector by the kinetic mixing with the visible Higgs D-term. In such a case, the mass-squareds m_+^2, m_-^2 may be positive provided they are small enough that $\Delta^2 > 0$. One motivation for this work is that such a case is difficult to justify in the case of gravity mediation; it is however not impossible, for example through fine-tuning of the parameters or through sequestering. We shall in the section 4 examine this case, still assuming that the gravitino is not the LSP.

2.5 Dark matter candidates

The model above contains essentially two different dark matter candidates: a Majorana fermion and a Dirac one.[2] Neglecting the effect of kinetic mixing with the visible neutralino, the fermion mass matrix in the basis $(\tilde{\lambda}, \tilde{h}_+, \tilde{h}_-, \tilde{s})$ corresponding to hidden gaugino, hidden higgsinos and

---

[1]We ignore the effect on the running of the kinetic mixing, since such terms always enter suppressed by $\mathcal{O}(\chi^2)$ [19]. Of course, it would be interesting to include all of these effects, but the hidden sector running would then be (of course very weakly) dependent upon the visible sector parameters and we leave this to future work.

[2]We are ignoring the possibility of scalar dark matter since, although the model as we have written it contains stable scalars, we expect the symmetries protecting them to be broken at some higher order in the potential allowing them to ultimately decay.
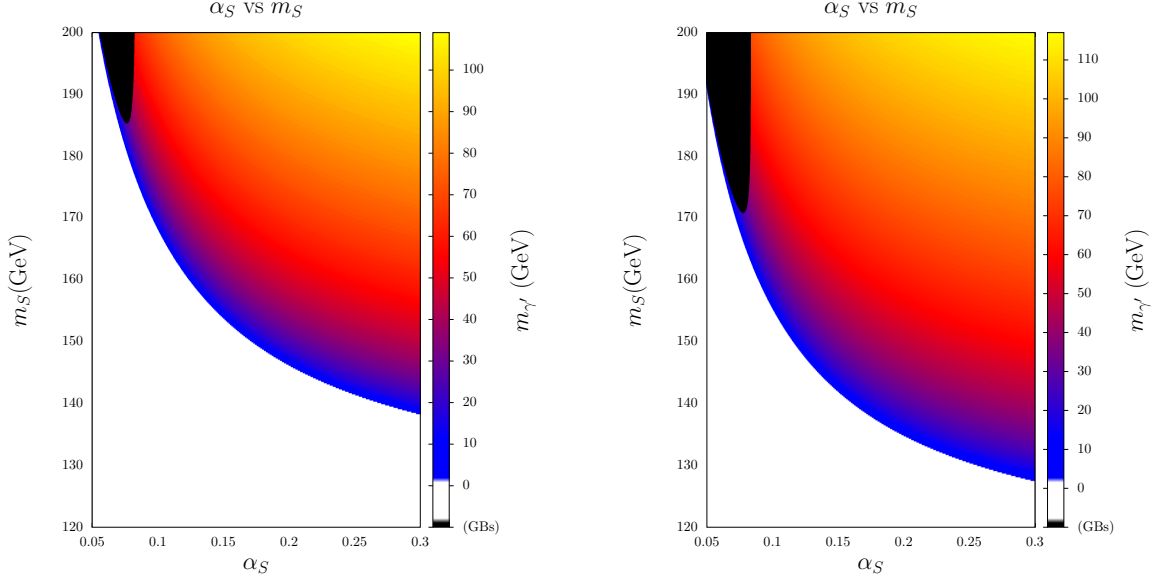
Figure 1: Hidden photon mass induced by radiative hidden gauge symmetry breaking, scanned over m_S and $\alpha_S \equiv \frac{\lambda_S^2}{4\pi}$. In both, $m_H = A_S = 100$ GeV, $\alpha_h = 0.0417$. Left: $M_\lambda = 71$ GeV, right: $M_\lambda = 50$ GeV. All values given at 10^{16} GeV. The black region shows no stable symmetry breaking.

hidden singlino is given by

$$
\mathcal{M}_f = \left(\begin{array}{cccc} M_\lambda & m_{\gamma'} & 0 & 0 \\ m_{\gamma'} & 0 & 0 & 0 \\ 0 & 0 & 0 & \Delta \\ 0 & 0 & \Delta & 0 \end{array} \right). \tag{2.10}
$$

The Majorana particle is formed from diagonalising the $\tilde{\lambda}, \tilde{h}_+$ states; in the case of a large M_λ this leads to a see-saw effect and a low mass. We shall refer to this state as "$\tilde{o}_1$", micrOMEGAs notation for the lightest odd particle. Clearly there will therefore always be a fermion lighter than the hidden gauge boson (to avoid this fate we would need to add a mass for the hidden singlino). In order for the Dirac fermion formed from $\tilde{h}_-, \tilde{s}$ to be the lightest state we would need $\lambda_S < \sqrt{2}g_h$ and for the Majorana mass M_λ to be rather small at the high energy scale (this could happen for example in a string model where the modulus corresponding to the gauge coupling does not obtain an F-term) although it is somewhat suppressed in running down to the low scale. Hence the Dirac fermion scenario is not compatible with radiative-breaking models, but presents an attractive candidate for the visible sector induced breaking. We shall refer to this state as "$\tilde{o}_7$".

In a complete analysis including the couplings and annihilation cross-sections, it is necessary to take the mixing with the visible neutralino into account; this we do in appendix section B.2.

6

3 Constraints and discovery potential

There are already a wealth of constraints on the parameter space of models with dark forces and hidden matter that we must apply in our search over models. However, there are also future experiments which will have the potential to rule further regions out - or make a discovery. In this section we summarise these current and future constraints, and illustrate them by application to a toy model.

3.1 Limits on the hidden photon

Constraints from electroweak precision tests (EWPT) are used as have been presented in [39], where the strongest constraint is provided by the mass of the Z for most of the parameter space. In the following plots of χ vs $m_{\gamma'}$ this is shown as a long-dashed approximately horizontal blue line excluding roughly $\chi \gtrsim 3 \times 10^{-2}$. Another constraint comes from the muon anomalous magnetic moment [51] and is dominant for $m_{\gamma'} < 1$ GeV: in most of the following plots of χ vs $m_{\gamma'}$ this is a long-short-dashed brown line at low masses and $\chi > 10^{-2}$. There are model dependent constraints from BaBar searches [39] that might be the most constraining in the region 0.2 GeV $\lesssim m_{\gamma'} \lesssim$ 10 GeV but only apply if the γ' can not decay into hidden sector particles; in most following plots of χ vs $m_{\gamma'}$ this is a dashed dark purple line at low masses below 10 GeV and $\chi \sim 2 \times 10^{-3}$. These do apply for most of the supersymmetric models we are considering, where the mass of the γ' and hidden matter are similar - preventing a decay to the hidden sector. However, if the hidden photon can decay to hidden matter, then there is instead a much weaker constraint from the Z width; we require

$$\frac{\Gamma(Z \to \text{hidden})}{\Gamma(Z \to \nu\bar{\nu})} \lesssim 0.008 \tag{3.1}$$

which for a single hidden Dirac fermion of mass $M_X < M_Z$ and unit charge under the hidden U(1) corresponds to (see also [52])

$$8c_W^2 s_W^2 (\frac{s_\phi}{c_\epsilon})^2 \left(\frac{g_h^2}{e^2}\right) (1 + 2\frac{M_X^2}{M_Z^2})\sqrt{1 - 4\frac{M_X^2}{M_Z^2}} \lesssim 0.008 \tag{3.2}$$

where c_W, s_W are the usual cosine and sine of the weak mixing angle respectively, s_ϕ is defined in equation (C.7); for $M_X \ll M_Z$ this simplifies to $\chi g_h \lesssim 0.04$. Clearly for a small number of hidden particles (and $g_h < 1$) this is a weaker constraint than the measurement of the Z mass.

For $m_{\gamma'}$ below 1 GeV there are additional constraints from fixed target experiments [53, 54]. Not only are there limits on the kinetic mixing for very light hidden photons, but excitingly there are also dedicated experiments planned (and partly already running) that can further probe this parameter space with real discovery potential. The estimated sensitivities of those experiments are shown in the plots for the toy model in section 3.3. There are two fixed target experiments (MAMI [55] and MESA) in Mainz, three (APEX [56, 57], DarkLight [58] and HPS) at JLab and one (HIPS) [59] at DESY.

3.2 Limits from dark matter

There are further constraints arising on the dark matter particle, its mass and its interactions. First of all, the dark matter particle should not have a relic abundance in excess of the one

measured by WMAP [60]. This is a very strict limit and translates to a limit on the dark matter (DM) annihilation cross section. We compute the dark matter relic abundance using micrOMEGAs where we have implemented our model. However, while there is an upper limit on the relic abundance, there is no objection to having a dark matter candidate whose abundance is lower than the one measured. In this case, it would than only be a part of the total dark matter (we shall refer to this as subdominant DM) and the remaining dark matter density would consist of other particle(s) such as an axion or axion-like particle whose phenomenology is not the subject of this article - we shall simply assume in such cases that the direct detection cross-sections and interactions with the hidden sector of the additional dark matter are both negligible. In our plots we show parameter points that give an abundance in agreement with the WMAP value in dark green and ones where the DM is subdominant in light green.

Additional constraints apply to the dark matter particle and its scattering cross section on nuclei. It is necessary to distinguish spin-dependent (SD) and spin-independent (SI) scattering. Dependant on whether the dark matter particle is a Majorana or Dirac fermion it has either dominantly SD or SI interactions respectively. Current limits from direct dark matter detection experiments are strongest for SI scattering cross sections ($\sim 10^{-42}$ cm^2) while SD cross sections only start to be excluded at the 10^{-38} cm^2 level.

For the low dark matter masses (~ 10 GeV) we are interested in, the most relevant constraints come on the SI side from XENON and CDMS. However due to the signal claims from DAMA and CoGeNT,[3] there has been a large debate on the reliability of those constraints, especially at low dark matter masses close to the energy threshold of the experiments. There are also large astrophysical (halo model, dark matter velocity, local dark matter density) and nuclear physics uncertainties that should be taken into account. Even though XENON and CDMS claim to rule out most of the DAMA and CoGeNT preferred regions, the positive signals remain and there have been various studies of how to reconcile those different results. [4] We adapt the analysis of [66] which made a systematic scan taking into account the various uncertainties. There it is found that depending on the halo model some of the CoGeNT and sometimes even DAMA preferred region is consistent with the exclusions from XENON and CDMS. For the details of the different halo models see [66]; we will mostly use their so-called SMH (Standard Model Halo) and in a few cases show the differences that arise when changing for example to a NFW or an Einasto profile.

We strictly apply the XENON100 and CDMSSi constraints derived in [66] to the SI scattering cross sections and only show points that are not excluded by any of the two experiments. In the plots of $\sigma_{\rm SI}$ vs $m_{\rm DM}$ in section 4 (see figures 7, 11 and 12) the CDMS limit is shown as a dashed turquoise line while XENON is a blue dash-dotted line (in the plots of section 3.3 the additional constraints due to accelerator experiments are shown as grey areas). For most halo models CDMS is more constraining at lower masses than XENON.

Regarding SD scattering there are several direct detection experiments sensitive to the low dark matter masses we are interested in. Until June, Picasso for the lightest and COUPP for the slightly larger masses were the most constraining experiments [67]. There is also a quite strong limit from Super-K using neutrino fluxes produced by dark matter annihilation in the Sun

---

[3]We have not explicitly included the CRESST signal in our search. One of their two signal regions is roughly compatible with both DAMA and CoGeNT signals, although this is still subject to astrophysical uncertainties.

[4]One interesting possibility is to allow isospin-dependent interactions with just the right behaviour to suppress the interaction cross-section with xenon nuclei [61–65]. We simply note that, although in the case of hidden Dirac fermions the interaction is almost entirely with protons rather than neutrons, in our models this tuning is not possible.

which however only applies to dark matter masses above 20 GeV (only neutrino-induced upward through-going muons have been used in this analysis which leads to a quite high energy threshold and therefore a sensitivity only to larger DM masses) [68]. Very recently a new direct detection experiment SIMPLE [69] has published a limit on the SD scattering cross section which in the low mass range is one order of magnitude stronger than previous experiments (for a critique of their limit see [70] and the collaboration's response [71]).

In the following analysis we use the pre-SIMPLE constraints as strict exclusions and show only points consistent with those limits. As there has been criticism of SIMPLE's limit we will not apply this universally but rather show how our results change when taking it into account. In the SD plots the exclusion lines for the different experiments are as follows: SIMPLE brown short-dashed line, Super-K black long-dashed line, PICASSO orange almost solid line, COUPP2011 turquoise dash-dotted line, COUPP2007 blue solid line, KIMS green long dashed line.

In the plots the scattering cross section on protons both in the SD and the SI is given. For SI scattering the reason for this is that the dark matter couples via the kinetic mixing and thus to the charge of the nucleon. This is not the case for SD scattering and both cross sections on neutrons and protons are roughly the same, however the one on protons is shown.

Those constraints on the scattering cross section can strictly only be applied to particles that actually constitute the entire dark matter density. If the dark matter is subdominant however, the limits on its scattering cross section have to be rescaled accordingly: the local density ρ_ψ of a dark matter candidate ψ relates to the local total DM density ρ_{DM} as their abundances

$$\frac{\rho_\psi}{\rho_{\mathrm{DM}}} = \frac{\Omega_\psi}{\Omega_{\mathrm{DM}}} \tag{3.3}$$

and so do the limits that are set by direct detection (DD) experiments. Thus an experimental bound on σ_{DD} translates into an actual bound on the scattering cross section σ_ψ of ψ as

$$\sigma_\psi = \sigma_{\mathrm{DD}} \frac{\Omega_\psi}{\Omega_{\mathrm{DM}}}. \tag{3.4}$$

This means that direct detection constraints on the scattering cross section become less potent for subdominant DM particles.[5]

3.3   Application to toy model

To illustrate the above constraints/future experimental reach, and more importantly provide a comparison to the more complete model of section 2 that we shall investigate in section 4, here we shall consider a toy model. This is the simplest possible dark sector: a Dirac fermion ψ with unit charge only under the (massive) hidden U(1). We shall not include any Higgs sector - the U(1) could, after all, naturally have a GeV scale mass via the Stückelberg mechanism [23, 27] - so we will not consider how the dark matter particle becomes massive. This is essentially the model considered in [41–45] except that we shall insist on the relation (2.4); the parameters are the dark matter mass m_{DM}, hidden photon mass $m_{\gamma'}$, kinetic mixing χ and the tuning parameter κ.
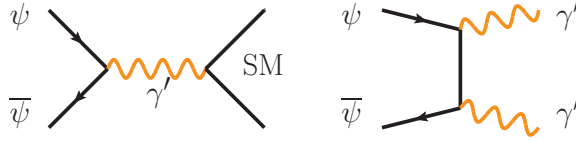
Figure 2: Annihilation diagrams: s-channel annihilation on the left, resonant at $m_{\gamma'} = 2m_{\rm DM}$; t-channel on the right, accessible and dominant when $m_{\rm DM} > m_{\gamma'}$.

3.3.1 Constraints and future searches

The DM can annihilate through and/or into hidden photons according to the diagrams shown in figure 2. Whereas the left diagram is possible for all DM masses, the right one is kinematically only accessible when $m_{\rm DM} \geq m_{\gamma'}$. The left diagram also leads to a resonant enhancement of the annihilation cross section and accordingly to a dip in the relic abundance for $m_{\gamma'} = 2m_{\rm DM}$. This can been seen in figure 3 where we show the relic abundance for a dark matter mass of 6 GeV (two top plots) and 7 GeV (bottom) in function of the kinetic mixing χ and the hidden photon mass $m_{\gamma'}$. The grey areas are those excluded by beam dump experiments (the curves on the left side of the plot) and muon and electron anomalous magnetic moment (top left corner of the plot) and the BaBar search as well as EWPT for large kinetic mixing and hidden photon mass. The thin dark green band is the region which gives the correct WMAP abundance while in the light green areas the DM candidate is subdominant. The white regions are excluded since they give a too large relic abundance. For very small hidden photon masses annihilation proceeds only via the left diagram and is essentially independent of $m_{\gamma'}$. Therefore the relic abundance is given by the kinetic mixing only which itself is determined by the hidden gauge coupling up to a factor κ; the effect of varying κ on the relic abundance is shown in figure 3 where the two extreme cases of its range are used. The coloured lines with named labels represent future searches, which as can be seen from the plot will probe portions of the interesting parameter space.

This DM particle can also scatter elastically on nuclei. As it is a Dirac fermion, this process is spin-independent and the corresponding cross sections can be compared to the positive observations of DAMA and CoGeNT. The results in figure 3 are given for the Standard Halo Model (SMH) where part of the CoGeNT allowed region is not excluded by the other experiments (CDMS and XENON). The dark matter mass of 6 GeV used in the two top plots is not constrained by CDMS or XENON. The band in purple corresponds to the 90% (lighter purple) and 99% (darker purple) contours where the correct cross section for CoGeNT can be obtained. At the place where this band overlaps with the dark green region, the DM candidate that fits CoGeNT is also providing all of the dark matter in the universe. In the larger part however, where the purple band is on top of the light green area, the DM particle explains the CoGeNT signal while only contributing subdominantly to the total DM.

For the 7 GeV dark matter the scattering cross section is constrained by CDMS (still below the reach of XENON) which is shown as a turquoise line excluding all the parameter space above it (where there are dotted vertical lines). Where the CDMS exclusion bound enters the WMAP allowed, coloured, region the limit is rescaled as described above to correspond to the appropriate dark matter density. However, outside of this region it is not rescaled - the straight line shown

---

[5]This is obviously based on the reasonable assumption that the local DM has the same content of different DM contributions as averaged over the whole universe.
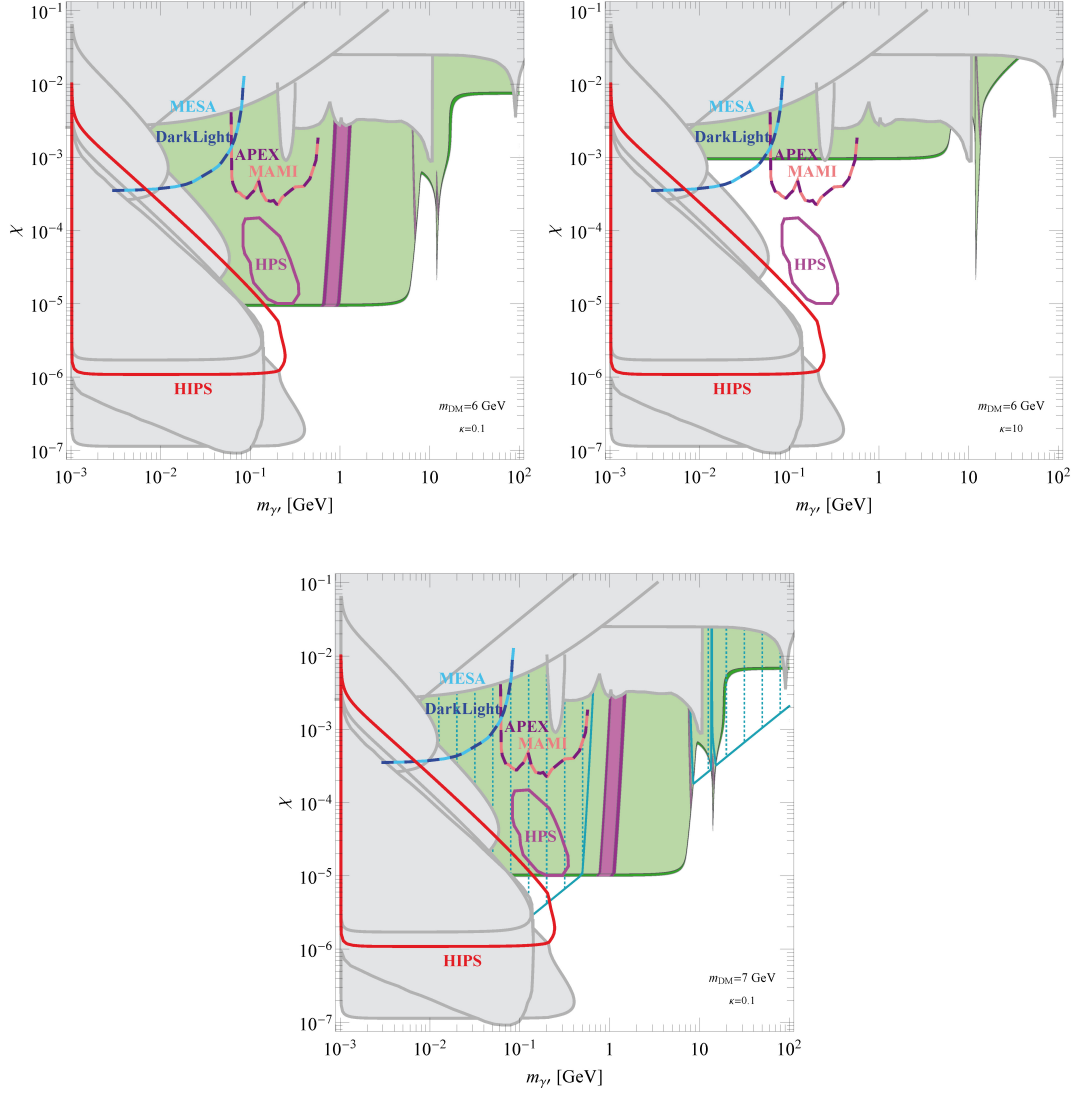
Figure 3: Dark matter (DM) relic abundance and direct detection (DD) cross section in agreement with CoGeNT for a dark matter mass of 6 GeV (top) and 7 GeV (bottom) and the two extreme values of the range in which the free parameter κ can vary (only for 6 GeV). The Standard Halo Model (SMH) has been used. The grey regions are excluded, the coloured lines correspond to sensitivities of future planed fixed target experiments. Dark green regions give the correct relic abundance, light green is subdominant DM, white is overabundant and therefore excluded. In the purple area, the cross sections are such that they can explain the CoGeNT observation. The turquoise line is the CDMS bound which excludes all the dashed shaded area above the line.

corresponds to the behaviour for a constant dark matter density equal to that observed. This accounts for the sudden change in gradient. Note that relation (2.4) has a significant effect upon the behaviour of this bound. Outside of the WMAP allowed region, i.e. when we are applying the CDMS bound for a fixed dark matter density, the corresponding cross-section follows a contour of
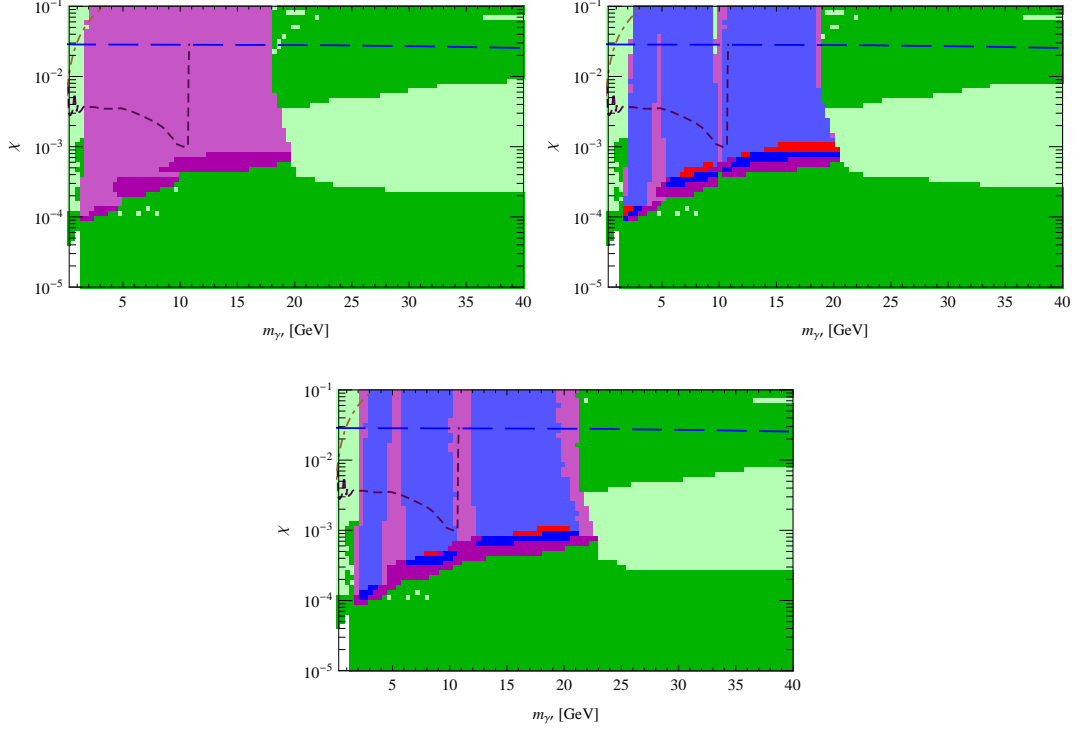
11

Figure 4: Scan over hidden photon mass, kinetic mixing and hidden Dirac fermion mass over the range from 0.8 GeV to 20 GeV, using the Standard Halo Model. Dark coloured regions indicate that the correct relic abundance can be found, lighter colours indicate that the hidden fermion is a subdominant dark matter candidate. Green regions are thus simply WMAP allowed, but also shown are regions where the direct detection cross section can explain the signal from either CoGeNT (purple), DAMA (red) or both at the same time (blue). The parameter κ has been fixed to 1. For subdominant DM the scattering cross sections have been rescaled. All points shown in the figure are in agreement with all direct detection constraints. The constraint from electroweak precision tests is shown as the almost horizontal blue long dashed line, the (model dependent) BaBar limit is shown as a dark dashed line and from the muon $g - 2$ dash-dotted.

$\chi \propto m_{\gamma'}$, rather than $\chi \propto m_{\gamma'}^2$ which we would find if we were instead keeping g_h constant. This arises since the cross-section behaves as

$$\sigma_{\text{DD}} \propto \frac{\chi^2 g_h^2}{m_{\gamma'}^4} \propto \frac{\chi^4}{m_{\gamma'}^4}. \tag{3.5}$$

This explains the straight line portion of the CDMS bound in the $\log - \log$ plots of figure 3. Note how this changes when we take rescaling into account: since the thermal-averaged ψ-$\overline{\psi}$ annihilation cross-section multiplied by speed $\langle \sigma_{\text{Ann}} v \rangle$ for fixed dark matter and hidden photon mass is proportional to either $g_h^2 \chi^2$ or g_h^4, which according to equation (2.4) translates into $\langle \sigma_{\text{Ann}} v \rangle \propto \chi^4$, and as the relic density is propotional to $1/\langle \sigma_{\text{Ann}} v \rangle$, we find

$$\sigma_\psi \propto \frac{\chi^4}{m_{\gamma'}^4} \frac{1}{\langle \sigma_{\text{Ann}} v \rangle} \propto \frac{1}{m_{\gamma'}^4}. \tag{3.6}$$

Hence the rescaled CDMS exclusion bound is approximately a vertical line on the plot, as can be seen in figure 3 where the turquoise line meets the green band.

3.3.2 Scanning over dark matter masses

To fully examine the parameter space of these models, we performed a scan over the mass of the particle ψ for values between 0.8 and 30 GeV (in steps of 0.2 GeV) while also varying the kinetic mixing and hidden photon mass. The resulting scatter plots are shown in figure 4 for three different halo models (for details of the halo models see [66]). For these plots the parameter κ was fixed to its central value of one. The colouring is as follows: dark shades correspond to the dark matter candidate producing the observed relic abundance, lighter shades indicate it is subdominant; green regions do not correspond to an experimental signal but are not excluded; purple corresponds to explaining the CoGeNT signal; the DAMA signal is explained in the red regions; CoGeNT and DAMA signals are explained simultaneously in the blue regions. For the Standard Halo Model (SMH), the CoGeNT and DAMA signal regions do not overlap, and this is reflected in the absence of blue in our SMH plots. However for the Einasto and NFW halo models there is a small region of overlap in mass-cross-section space for the signal regions, which translates into blue regions of our plots with those halo models. However, in the following section we shall use mostly the standard halo model; the choice of halo has a more dramatic effect on the presence (or otherwise) of overlap of the signal region than the allowed parameter space of our models.

4 Analysis of a supersymmetric dark sector

In this section we describe the results of a scan over the parameter space of the model of section 2, constrained by dark matter abundance and direct detection cross-sections. This was achieved by implementation of our models in micrOMEGAs [46–50] using LanHEP [72–76]. We included all of the interactions between the hidden and visible sector including the neutralino mixing (described in appendix section B.2) and Higgs portal term (described in appendix E) which we believe to be novel results; as a result, there is some dependence on the visible sector spectrum and couplings. Since we were investigating the effects of gravity mediation, and for minimality, we chose the visible sector to consist of the MSSM with a Higgs mass above the LEP bound and the lightest visible sector neutralino in the range 100 to 200 GeV; the effect of changing the spectrum within these ranges leads to quantitative changes of a few percent, but not qualitative ones.

4.1 Radiative breaking domination

Here we perform a scan over λ_S, χ and $m_{\gamma'}$ in order to find parameter combinations which give a light dark matter (DM) candidate (target DM masses in the range between 0.8 and 20 GeV) which as mentioned in section 2.5 we find to be exclusively a Majorana fermion $\tilde{o}_1$. We insist that λ_S and the hidden gauge coupling inferred from χ remain perturbative; this places an upper limit upon χ via equation (2.4). We are interested in light hidden gauge bosons, so we choose a maximum value of $m_{\gamma'}$ of 40 GeV. The low energy parameters are found by choosing boundary conditions at the high energy scale (10^{16} GeV) and running down; this ensures that we have bona fide consistent models at the low energy scale, rather than choosing the parameters completely ad hoc. This search uses the RGE engine from SoftSUSY [77].
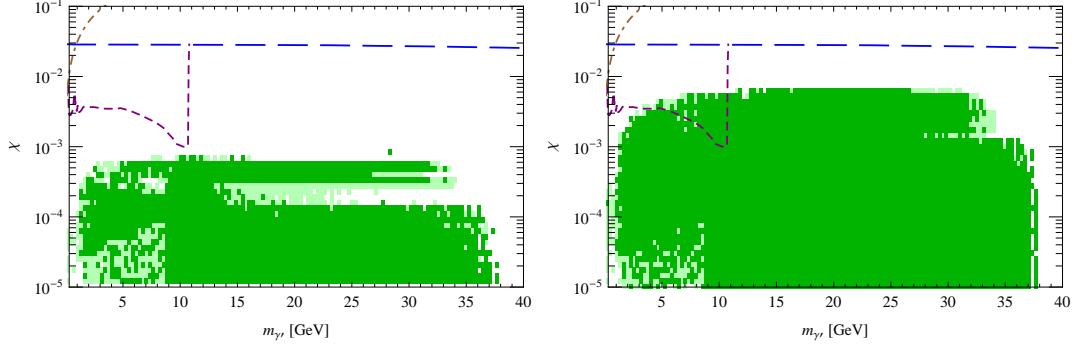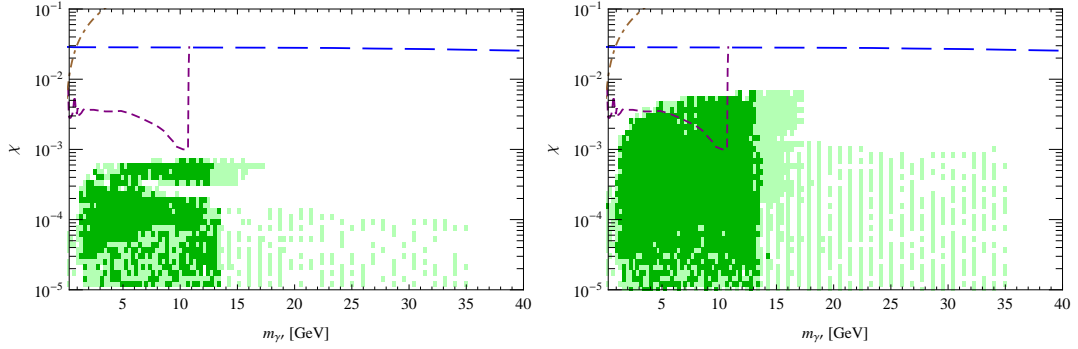
Figure 5: Allowed space of models with radiatively induced breaking. Dark green areas allow for the correct dark matter relic density; light green for subdominant dark matter. The Standard Halo Model (SMH) has been used, and all constraints imposed **except for** the SIMPLE exclusion limit. *Left:* $\kappa = 1$, *right:* $0.1 \leq \kappa \leq 10$.

Figure 6: Allowed space of models with radiatively induced breaking. Dark green areas allow for the correct dark matter relic density; light green for subdominant dark matter. The Standard Halo Model (SMH) has been used, and all constraints imposed **including** SIMPLE exclusion limit. *Left:* $\kappa = 1$, *right:* $0.1 \leq \kappa \leq 10$.

We then input the results of the scan into micrOMEGAs to obtain the corresponding relic abundance and scattering cross sections. Results for kinetic mixing against hidden photon mass are shown in figures 5 and 6 for $\kappa = 1$ and for a scan over κ in the range 0.1 to 10. Depending on whether the relic abundance corresponds to the total DM abundance the points are shown in dark green or in light green if it is subdominant. Clearly allowing for variation in κ has a large effect on the allowed space of models, in stark contrast to the toy model in section 3.3 where the parameter space could be filled without varying κ.

The spin-dependent and spin-independent direct detection cross-sections are shown in figure 7, where κ has been scanned over and we again use the rescaling procedure for subdominant dark matter. The dark matter particle considered in this subsection $\tilde{o}_1$ is a Majorana fermion and therefore has greatly suppressed spin-independent scattering on nuclei (so there is little chance of explaining the DAMA or CoGeNT signals via spin-independent scattering with such a model); however, the obtained spin-dependent cross sections are quite large and some are even already
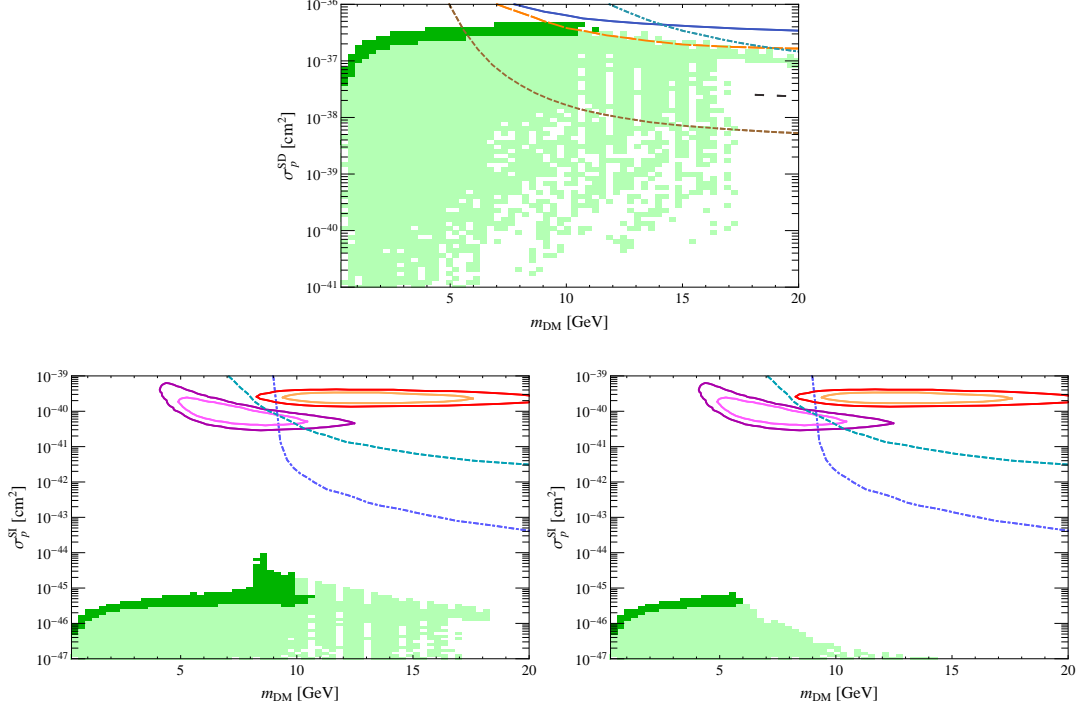
14

Figure 7: Direct detection cross-sections for radiatively induced breaking, using SMH, scanning over $0.1 \leq \kappa \leq 10$. *Top:* spin-dependent scattering (σ^{SD}) with experimental exclusion contours, SIMPLE shown as the lowest-lying, brown, curve; *left:* spin-independent scattering (σ^{SI}) without SIMPLE limit; *right:* spin-independent scattering (σ^{SI}) with SIMPLE limit.

excluded by current experiments (the experiments were mentioned in section 3). The most stringent constraint arises from the SIMPLE experiment which cuts out many parameter points for dark matter masses above ~ 6 GeV; the effect of this is illustrated by showing the parameter scan before SIMPLE is included in figure 5 and afterwards in figure 6. Since the spin-dependent and spin-independent cross-sections are related, the SIMPLE limit removes a large portion of the parameter space with larger values of *spin-independent* scattering direct-detection cross-sections; this is illustrated in figure 7, which shows on the top plot all the found spin-dependent cross-sections and the experimental bounds, then on the left and right plots the corresponding spin-independent cross-sections without and with the SIMPLE bound respectively - the missing models on the right plot are those that lie above the SIMPLE exclusion contour for spin-dependent scattering.

As mentioned above, the fact that the hidden sector dark matter candidate is a Majorana fermion leads to extremely small spin-independent scattering cross sections. They do however obtain a contribution from the Higgs portal term, which in supersymmetric theories is always present. We describe this in detail in appendix E, where we also derive a simple approximation for the contribution of the Higgs portal term which agrees well with the results seen in figure 7:

$$\sigma_N^{\text{SI, Portal}} \sim 10^{-45} \text{cm}^2 \times \left(\frac{m_{\tilde{o}_1}}{m_N + m_{\tilde{o}_1}} \right)^2 \left(\frac{\chi s_W}{0.001} \right)^2 \left(\frac{\text{GeV}}{m_{\gamma'}} \right)^2 . \tag{4.1}$$

There is also a somewhat smaller and more spectrum-dependent contribution from squark ex-

change. Here the spin-independent nuclear cross-sections are very similar for protons and neutrons; that for protons is shown for direct comparison with the next subsection.

Our results in this subsection are largely independent of the halo model applied to the spin-independent scattering limits, as the corresponding cross-sections are much below the experimental reach.

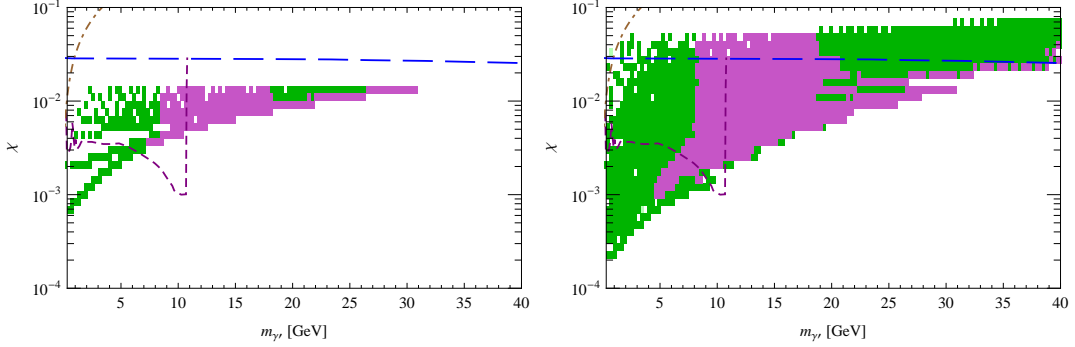## 4.2 Visible sector induced breaking

Figure 8: Allowed space of models with visible-sector induced breaking, showing dark green areas where the correct dark matter relic abundance can be found and light purple where the CoGeNT signal can be explained with a subdominant dark matter candidate. The Standard Halo Model (SMH) has been used, and all constraints imposed including the SIMPLE exclusion limit. *Left:* $\kappa = 1$, *right:* $0.1 \leq \kappa \leq 10$.

Here we implement a scan for visible sector induced breaking, by scanning over parameters at the low energy scale. As in the previous subsection, we insist on perturbativity for λ_S and g_h, and take a maximum value of $m_{\gamma'}$ of 40 GeV. However, the soft supersymmetry breaking masses are chosen to be small, as may be induced in gauge mediation or sequestering of the hidden sector. Phenomenologically then, the results of this subsection can be considered to be a detailed examination of the model of [19], but with a large gravitino mass and kinetic mixing respecting the relation (2.4).

As mentioned in section 2.5, we can have either of two dark matter candidates, depending on the particular low energy parameters: either the Majorana fermion $\tilde{o}_1$ or a Dirac fermion $\tilde{o}_7$. For both cases we again use micrOMEGAs to compute the relic abundance and the scattering cross sections. The space of models in the kinetic mixing-hidden photon mass plane (all points shown are in agreement with all direct detection exclusions, including SIMPLE) are shown in figures 8 and 9; the colour code is identical to the scatter plots in the toy model of section 3.3 and the different experimental constraints are explained in the constraints section 3 (sensitivities correspond to DAMA and CoGeNT 90% and 99% contours as mentioned earlier). Figure 8 demonstrates the expansion in the parameter space by allowing a varation in κ; both $\kappa = 1$ and $0.1 \leq \kappa \leq 10$ are plotted, for the Standard Halo Model (SMH). Figure 9 shows the effect of changing the halo model: here we find subdominant explanations for separately DAMA and CoGeNT signals, and both simultaneously, which appear as light red, purple and blue regions respectively; simultaneously explaining both signals is only possible for certain halo models other
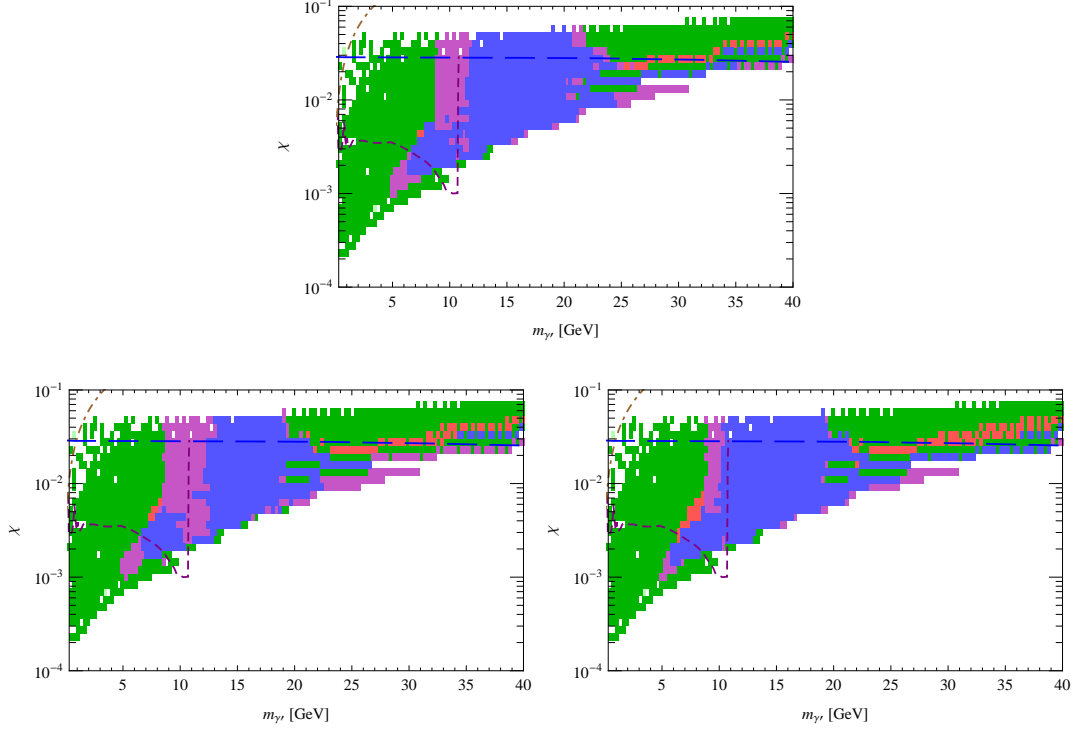
16

than SMH.

Figure 9: Allowed space of models with visible-sector induced breaking, scanned with $0.1 \leq \kappa \leq 10$, showing different halo models including the SIMPLE limit: *top:* NFW halo model, *left:* Isothermal halo model, *right:* Einasto halo model. Here the red region shows the space explaining the DAMA signal, the purple region explains the CoGeNT signal, and the blue explains both DAMA and CoGeNT, all signal regions having a subdominant dark matter density.

The resulting parameter points in figures 8 and 9 show a very similar behavior to the toy model (see figure 4) as here the dark matter candidate can also be a Dirac fermion. The main difference is that the models here never permit annihiliation via the t-channel diagram - since the dark matter particle can never be heavier than the hidden gauge boson. Therefore the lower part of the plots is, in contrast to the toy model, empty as there it was filled by dark green points finding the correct relic abundance lying either just above the threshold for t-channel annihilation or the s-channel resonance (as we scan over the dark matter mass these resonances move through the plot through different values of $m_{\gamma'}$ and the whole range is covered). The coarser grid and small holes in the current scatter plots compared to the toy model arise from the fact that the parameter space can not be scanned as continuously as for the toy-model.

The spin-dependent cross-sections are shown in figure 10, which are only appreciable when the Majorana fermion $\tilde{o}_1$ is the dark matter candidate. The spin-independent cross-sections for the Standard Halo Model are shown in figure 11, where the effect of scanning over the parameter κ on the parameter space is illustrated by showing plots with $\kappa = 1$ and $0.1 \leq \kappa \leq 10$. There are two disjoint regions corresponding to whether the dark matter candidate is the Majorana fermion $\tilde{o}_1$ (lower region) or Dirac, $\tilde{o}_7$ (upper region). As in the radiatatively-induced breaking case the

17

Majorana fermion has a small spin-independent cross-section of 10^{-47} to 10^{-45} cm^2. In contrast to this, the spin-independent scattering cross section of the Dirac fermion $\tilde{o}_7$ is in the range of current direct detection experiments, and may explain the signal due to CoGeNT and DAMA via a subdominant dark matter component. Hence we show the effect of the different halo models in figure 12, where simultaneous explanations of both signals are possible.
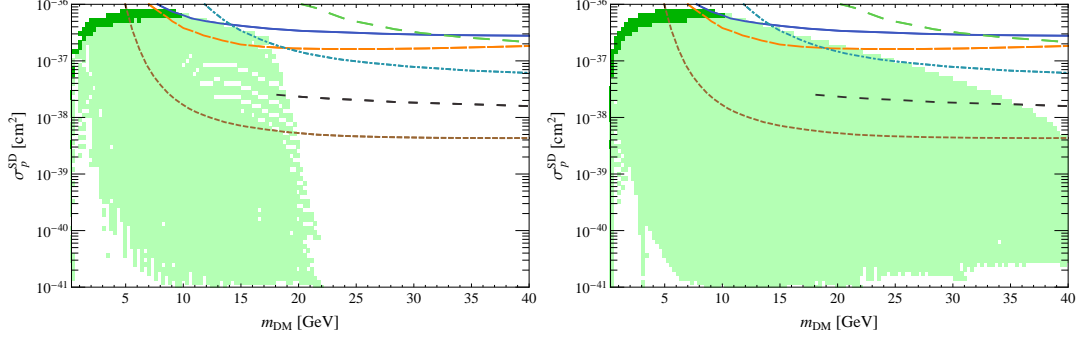

Figure 10: Spin-dependent cross-sections for visible-sector induced breaking, with the exclusion contours from direct detection experiments shown (the lowest lying, brown, line is due to SIMPLE). Here only the Majorana dark matter candidate $\tilde{o}_1$ is shown (the cross-sections due to an $\tilde{o}_7$ candidate are too small to appear). The SMH has been used. *Left:* $\kappa = 1$, *right:* $0.1 \leq \kappa \leq 10$.
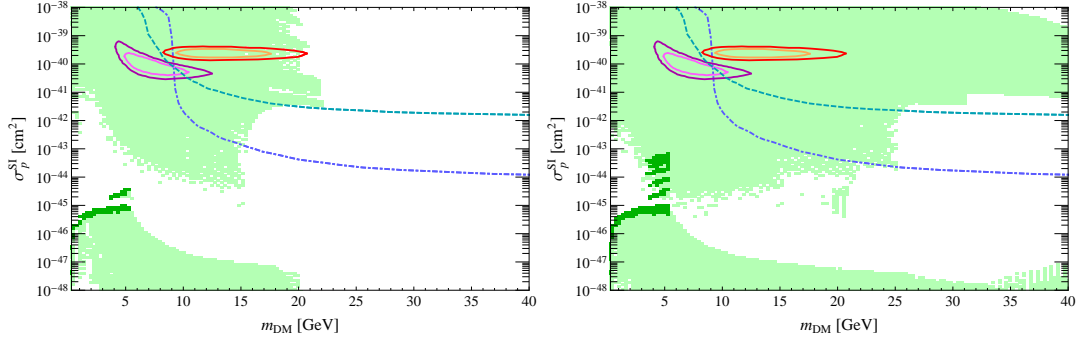

Figure 11: Spin-independent cross-sections for visible sector induced breaking using the SMH and including SIMPLE limit. The signal contours from CoGeNT (purple) and DAMA (Red) are shown; the exclusion limits from CDMS and XENON100 are shown as the coloured curves. The plot splits into two disjoint green areas: in the upper, Dirac fermion $\tilde{o}_7$ is the dark matter candidate, while in the lower one it is the Majorana fermion $\tilde{o}_1$. *Left:* $\kappa = 1$, *right:* $0.1 \leq \kappa \leq 10$.

The Dirac fermion $\tilde{o}_7$ has almost no spin-dependent scattering on nuclei, so the effect of the SIMPLE exclusion limit only affects the Majorana fermion (lower) regions in the spin-independent scattering plots 11 and 12, while the parameter regions that are interesting for spin-independent scattering experiments and can explain the DAMA and CoGeNT signals remain untouched. The spin-independent cross-sections are those on protons; as described above, the interaction through kinetic mixing couples almost exclusively to the charge of the nucleon, so the spin-independent

scattering on neutrons essentially vanishes (for the Dirac fermion $\tilde{o}_7$). For the case of the Majorana fermion $\tilde{o}_1$, spin-independent scattering on protons and neutrons is of roughly equal magnitude as it preceeds via the Higgs portal and squark exchange (as in the previous subsection), but the plots also show only the cross section on protons. Spin-dependent scattering is also shown in figure 10 on protons only but as in the previous subsection the cross sections on neutrons are almost the same (for the Majorana case). For the Dirac fermion dark matter the spin-dependent scattering essentially vanishes both for protons and neutrons.
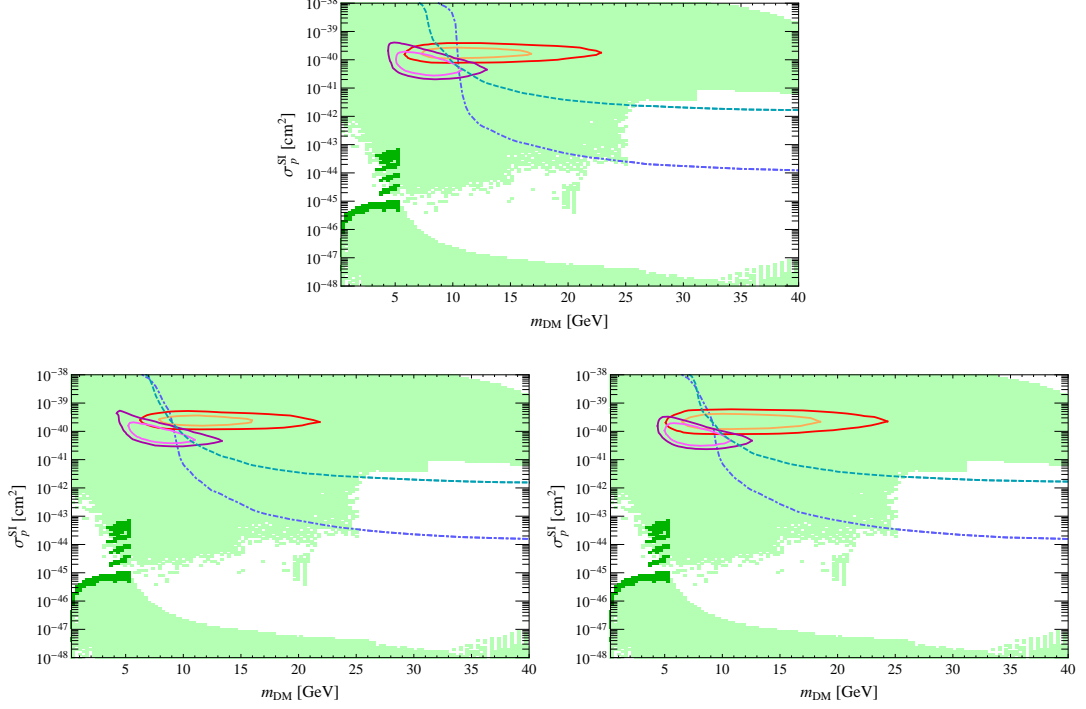

Figure 12: Spin-independent cross-sections for visible sector induced breaking including SIMPLE limit, scanning over $0.1 \leq \kappa \leq 10$, and showing three different halo models. *Top:* NFW, *left:* Isothermal, *right:* Einasto. The signal and exclusion regions are shown as in figure 11; as there, the upper and lower green regions in each plot corresond to dark matter candidates $\tilde{o}_7$ and $\tilde{o}_1$ respectively.

5 Conclusions and outlook

We have presented what we believe to be the first detailed examination of the dark matter relic abundance and direct detection cross-sections of a complete supersymmetric dark force model, emphasising the natural supersymmetric relationship between kinetic mixing and the hidden gauge coupling. In particular, we have included running from high energy gravity-mediated boundary conditions, and shown that interesting and viable models exist, in contrast to prior expectations. We have also examined the effect of neutralino mixing and the Higgs portal term, showing that the latter can contribute a small spin-independent cross-section for Majorana fermion dark matter candidates. We examined the model in the cases of both radiative and visible sector induced hidden

gauge symmetry breaking, and demonstrated the stark phenomenological constrasts between the two.

While the model can be used to explain the current dark matter signals observed by DAMA, CoGeNT and CRESST, this is not plausible in the case of radiative-induced breaking relevant for gravity mediation, where our motivation was to show that simple dark sectors are not excluded - the hidden U(1) may instead be detected in fixed target experiments, particularly if the hidden photon cannot decay to hidden matter (as in the reasonably generic case when the dark matter particle has mass near that of the hidden photon). However, this is certainly plausible if the model were to be extended, for example by allowing a supersymmetric mass for the singlet.

We hope that this work has paved the way for more detailed analysis of other supersymmetric dark sectors. In addition, there are several further possible avenues of work within the current model, for example by including the full loop corrections to the effective potential, and constraints from indirect dark matter searches (which is a work in progress although we believe them to be much less stringent than the direct searches). It would also be interesting to compare the signal from CRESST with those from DAMA and CoGeNT in the context of these models.

Acknowledgments

A Renormalisation group equations

Here we present the two-loop renormalisation group equations for the hidden-sector parameters $\alpha_S \equiv \lambda_S^2/4\pi, \alpha_h = g_h^2/4\pi, M_\lambda, m_+^2, m_-^2, m_S^2, A_S$, neglecting the effect of kinetic mixing. We define

$t \equiv \log \mu$:

$$
\frac{d\alpha_S}{dt} = \frac{1}{4\pi}[2\alpha_S(3\alpha_S - 4\alpha_h)] + \frac{1}{(4\pi)^2}[4\alpha_S(-3\alpha_S^2 + 2\alpha_S\alpha_h + 8\alpha_h^2)]
$$

$$
\frac{d\alpha_h}{dt} = \frac{1}{4\pi}[4\alpha_h^2] + \frac{1}{(4\pi)^2}[8\alpha_h^2(2\alpha_h - \alpha_S)]
$$

$$
\frac{dM_\lambda}{dt} = \frac{1}{4\pi}[4\alpha_h M_\lambda] + \frac{1}{(4\pi)^2}[8\alpha_h M_\lambda(4\alpha_h^2 - \alpha_S) + 8\alpha_h\alpha_S A_S]
$$

$$
\frac{dA_S}{dt} = \frac{1}{4\pi}[6\alpha_S A_S + 8\alpha_h M_\lambda] + \frac{1}{(4\pi)^2}[8A_S(\alpha_h\alpha_S - 3\alpha_S^2) - 8\alpha_h M_\lambda(\alpha_S + 8\alpha_h)]
$$

$$
\frac{dm_S^2}{dt} = \frac{1}{4\pi}[2\alpha_S(m_S^2 + m_+^2 + m_-^2 + A_S^2)]
$$
$$
+ \frac{1}{(4\pi)^2}\left[8\alpha_S(\alpha_h - \alpha_S^2)(m_S^2 + m_+^2 + m_-^2 + 2A_S^2) + 8\alpha_h\alpha_S(2M_\lambda^2 - 2M_\lambda A_S - A_S^2)\right]
$$

$$
\frac{dm_\pm^2}{dt} = \frac{1}{4\pi}[2\alpha_S(m_S^2 + m_+^2 + m_-^2 + A_S^2) - 8M_\lambda^2\alpha_h \pm 2\alpha_h(m_+^2 - m_-^2)]
$$
$$
+ \frac{1}{(4\pi)^2}\left[-8\alpha_S^2(m_S^2 + m_+^2 + m_-^2 + 2A_S^2) + 96\alpha_h^2 M_\lambda^2\right.
$$
$$
\left. + 8\alpha_h^2(m_+^2 + m_-^2) \pm 4\alpha(2\alpha_h - \alpha_S)(m_+^2 - m_-^2)\right] \tag{A.1}
$$

B Spectrum of the model

In this appendix we present the details of the low energy features of the model $W = \lambda_S SH_+H_-$. Once supersymmetry and the R-symmetry is broken the potential is

$$
V = |\lambda_S|^2(|SH_+|^2 + |SH_-|^2 + |H_+H_-|^2)
$$
$$
+ \frac{g_h^2}{2}(|H_+|^2 - |H_-|^2 - \xi)^2
$$
$$
+ m_+^2|H_+|^2 + m_-^2|H_-|^2 + m_S^2|S|^2
$$
$$
+ (\lambda_S A_S SH_+H_- + c.c.) \tag{B.1}
$$

We are assuming that no μ, B_μ terms are generated; these would introduce new scales into the theory. Although they could conceivably be generated by a Giudice-Masiero mechanism in analogy with the visible sector, we shall neglect this possibility.

B.1 Scalars

Defining $\Delta \equiv \sqrt{\lambda_S^2\xi - m_+^2\lambda_S^2/g_h^2}$, we have mass matrices in the $(H_+, H_+^\dagger)$ basis of

$$
\frac{1}{2}(H_+^\dagger\ H_+)\begin{pmatrix} g^2\Delta^2/\lambda_S^2 & g_h^2\Delta^2/\lambda_S^2 \\ g_h^2\Delta^2/\lambda_S^2 & g_h^2\Delta^2/\lambda_S^2 \end{pmatrix}\begin{pmatrix} H_+ \\ H_+^\dagger \end{pmatrix} \tag{B.2}
$$

which implies masses for the two components of $\sqrt{2}g_h\Delta/\lambda_S, 0$ at this level. The "massless" mode is the Goldstone boson that becomes the longitudinal component of the massive gauge field. The

$(H_-, H_-^\dagger, S, S^\dagger)$ system is more complicated; we find a mass matrix of

$$
\frac{1}{2}(H_-^\dagger \ H_- \ S^\dagger \ S)
\begin{pmatrix}
\Delta^2 + m_+^2 + m_-^2 & 0 & 0 & A_S^\dagger \Delta \\
0 & \Delta^2 + m_+^2 + m_-^2 & A_S \Delta & 0 \\
0 & A_S^\dagger \Delta & \Delta^2 + m_S^2 & 0 \\
A_S \Delta & 0 & 0 & \Delta^2 + m_S^2
\end{pmatrix}
\begin{pmatrix}
H_- \\ H_-^\dagger \\ S \\ S^\dagger
\end{pmatrix}. \quad \text{(B.3)}
$$

The above theory for non-zero ξ has a minimum at $\langle H_+ \rangle = \Delta/\lambda_S$ provided that Δ is real, and

$$
\begin{aligned}
0 \leq & m_-^2 + m_+^2 + m_S^2 + 2\Delta^2 \\
0 \leq & (m_-^2 + m_+^2 + \Delta^2)(m_S^2 + \Delta^2) - |A_S|^2 \Delta^2.
\end{aligned} \quad \text{(B.4)}
$$

In the case $A_S = 0, m_+^2 = m_-^2 < 0$ this translates simply to the condition that $\lambda_S^2 \geq 2g_h^2$.

B.2   Fermions and neutralino mixing

The fermion mass matrix in the basis $(\tilde\lambda, \tilde h_+, \tilde h_-, \tilde s)$ (neglecting the kinetic mixing of the gaugino with the neutralino) is given by

$$
\mathcal{M}_f =
\begin{pmatrix}
M_\lambda & m_{\gamma'} & 0 & 0 \\
m_{\gamma'} & 0 & 0 & 0 \\
0 & 0 & 0 & \Delta \\
0 & 0 & \Delta & 0
\end{pmatrix}. \quad \text{(B.5)}
$$

However, to properly compute the dark matter density we should take mixing of the fermions with the neutralino into account. The fields $\tilde h_-, \tilde s$ form a Dirac fermion that does not mix with any other fields. There will however be kinetic mixing of the bino with the hidden gaugino, and possibly mass mixing; writing these fields before the mixing as respectively $\tilde b, \tilde\lambda$ we can define

$$
\begin{aligned}
\tilde b =& \frac{1}{c_\epsilon} b \\
\tilde\lambda =& \lambda - t_\epsilon b,
\end{aligned} \quad \text{(B.6)}
$$

which then allows us to write the full neutralino mass matrix in the basis $(B_0, W_0, h_u^0, h_d^0, \tilde\lambda, \tilde h_+)$, including the standard Majorana masses for Bino and Wino $M_{1,2}$ but also a potential explicit mass mixing term $\mathcal{L} \supset -m_X \tilde b \tilde\lambda$ as

$$
\begin{pmatrix}
\frac{1}{c_\epsilon^2}[M_1 - s_\epsilon m_X + s_\epsilon^2 M_\lambda] & 0 & -M_Z s_W c_\beta/c_\epsilon & M_Z s_W s_\beta/c_\epsilon & \frac{1}{c_\epsilon}[m_X - s_\epsilon M_\lambda] & -m_\gamma' t_\epsilon \\
0 & M_2 & M_Z c_W c_\beta & -M_Z c_W s_\beta & 0 & 0 \\
-M_Z s_W c_\beta/c_\epsilon & M_Z c_W c_\beta & 0 & -\tilde\mu & 0 & 0 \\
M_Z s_W s_\beta/c_\epsilon & -M_Z c_W s_\beta & -\tilde\mu & 0 & 0 & 0 \\
\frac{1}{c_\epsilon}[m_X - s_\epsilon M_\lambda] & 0 & 0 & 0 & M_\lambda & m_\gamma' \\
-m_\gamma' t_\epsilon & 0 & 0 & 0 & m_\gamma' & 0
\end{pmatrix}
$$
$$\text{(B.7)}$$

C   Kinetic and mass mixing

Here we review the diagonalisation of the gauge fields and the subsequent coupling of the physical gauge bosons to matter fields.

Consider the lagrangian

$$
\begin{aligned}
\mathcal{L} = &-\frac{1}{4}\tilde{B}_{\mu\nu}\tilde{B}^{\mu\nu} - \frac{1}{4}\tilde{X}_{\mu\nu}\tilde{X}^{\mu\nu} + \frac{\chi}{2}\tilde{B}_{\mu\nu}\tilde{X}^{\mu\nu} - \frac{1}{4}\tilde{W}_{\mu\nu}\tilde{W}^{\mu\nu} + \frac{1}{2}\tilde{m}^2\tilde{X}_\mu\tilde{X}^\mu + \frac{1}{8}v^2(g_Y\tilde{B}_\mu - g_2\tilde{W}_\mu)^2 \\
&+ g_Y j_B^\mu \tilde{B}_\mu + g_2 j_W^\mu \tilde{W}_\mu + g_X j_h^\mu \tilde{X}_\mu \\
= &-\frac{1}{4}B_{\mu\nu}B^{\mu\nu} - \frac{1}{4}X_{\mu\nu}X^{\mu\nu} - \frac{1}{4}\tilde{W}_{\mu\nu}\tilde{W}^{\mu\nu} + g_2 j_W^\mu \tilde{W}_\mu + g_Y j_B^\mu B_\mu + \frac{1}{\sqrt{1-\chi^2}}(g_X j_h^\mu + \chi g_Y j_B^\mu)\tilde{X}_\mu \\
&+ \frac{\tilde{m}^2}{1-\chi^2}\frac{1}{2}X_\mu X^\mu + \frac{1}{8}v^2(g_Y B_\mu + \frac{g_Y\chi}{\sqrt{1-\chi^2}}X_\mu - g_2\tilde{W}_\mu)^2.
\end{aligned}
\tag{C.1}
$$

Then we rotate

$$
\begin{aligned}
\tilde{W}_\mu &\equiv s_W A_\mu + c_W(c_\phi Z_\mu + s_\phi \gamma'_\mu) \\
\tilde{B}_\mu &\equiv c_W A_\mu - s_W(c_\phi Z_\mu + s_\phi \gamma'_\mu) + \frac{\chi}{\sqrt{1-\chi^2}}(c_\phi \gamma'_\mu - s_\phi Z_\mu) \\
&= c_W A_\mu - (s_W c_\phi + \frac{\chi}{\sqrt{1-\chi^2}}s_\phi)Z_\mu + (\frac{c_\phi\chi}{\sqrt{1-\chi^2}} - s_W s_\phi)\gamma'_\mu \\
\tilde{X}_\mu &\equiv \frac{1}{\sqrt{1-\chi^2}}(-s_\phi Z_\mu + c_\phi \gamma'_\mu)
\end{aligned}
\tag{C.2}
$$

where c_W, s_W are the usual cosine and sine of the weak mixing angle respectively, c_ϕ, s_ϕ are the cosine and sine of an an angle ϕ to be determined below so that

$$
\begin{aligned}
\mathcal{L} \supset &-\frac{1}{4}F_{\mu\nu}F^{\mu\nu} + m_{\gamma'}^2\frac{1}{2}\gamma'_\mu(\gamma')^\mu + M_Z^2\frac{1}{2}Z_\mu Z^\mu \\
&+ eA_\mu\left[j_W^\mu + j_B^\mu\right] \\
&+ Z_\mu\left[g_2 c_W c_\phi j_W^\mu - (s_W c_\phi + \frac{\chi s_\phi}{\sqrt{1-\chi^2}})g_Y j_B^\mu - \frac{g_X s_\phi}{\sqrt{1-\chi^2}}j_X^\mu\right] \\
&+ \gamma'_\mu\left[g_2 c_W s_\phi j_W^\mu + (\frac{c_\phi\chi}{\sqrt{1-\chi^2}} - s_W s_\phi)g_Y j_B^\mu + \frac{g_X c_\phi}{\sqrt{1-\chi^2}}j_X^\mu\right].
\end{aligned}
\tag{C.3}
$$

We find, defining $x \equiv m^2/M_Z^2$:

$$
\begin{aligned}
\tan 2\phi &= -\frac{2s_W s_\epsilon c_\epsilon}{c_\epsilon^2 - s_W^2 s_\epsilon^2 - x} \\
\sin\phi &= \frac{s_W\chi}{1-x} + ...
\end{aligned}
\tag{C.4}
$$

In terms of these, we have the eigenvalues where m_+ corresponds to the physical Z mass, m_-

to the physical hidden photon mass:

$$m_\pm^2 = \frac{1}{2}\left[m^2 + \frac{M_Z^2}{\cos^2\alpha} \pm \sqrt{\left(\frac{M_Z^2}{\cos^2\alpha} + m^2\right)^2 - 4m^2 M_Z^2}\right]$$

$$m_+^2 = M_Z^2\left[1 + \frac{s_W^2\chi^2}{1-x} + ...\right]$$

$$m_-^2 = \tilde{m}^2\left[1 + \frac{(1 - s_W^2 - x)\chi^2}{1-x} + ...\right].$$

$$(C.5)$$

Thus the masses are only shifted at order χ^2.

Note that we can also write

$$m_+^2 = M_Z^2(c_\phi - s_W t_\epsilon s_\phi)^2 + \frac{\tilde{m}^2}{c_\epsilon^2}s_\phi^2$$

$$m_-^2 = M_Z^2(s_\phi + s_W t_\epsilon c_\phi)^2 + \frac{\tilde{m}^2}{c_\epsilon^2}c_\phi^2$$

$$(C.6)$$

and, defining $\hat{x} \equiv m_-^2/m_+^2 \approx x$ we have

$$\tan\phi = \frac{-(1-\hat{x}) \pm \sqrt{(1-\hat{x})^2 - 4s_W^2 t_\epsilon^2 x}}{2s_W t_\epsilon \hat{x}}.$$

$$(C.7)$$

D Goldstone boson mixing

Here we consider the effect of the mixing on the Goldstone bosons that are eaten, and what happens to the other fields. Assuming that the visible sector is the MSSM, and taking the hidden sector to be broken by a single complex scalar C, we have

$$\mathcal{L} \supset |\partial_\mu C - ig_h \tilde{X}_\mu C|^2 + |\partial_\mu H_u^0 - \frac{i}{2}(g_Y B_\mu - g_2 W_\mu^0)H_u^0|^2 + |\partial_\mu H_d^0 + \frac{i}{2}(g_Y B_\mu - g_2 W_\mu^0)H_d^0|^2 + V_{hid}(C) + V_{vis}(H)$$

$$= \frac{1}{2}(\partial_\mu C_I - m_h\tilde{X}_\mu)^2 + \frac{1}{2}(\partial_\mu C_R)^2 + \frac{1}{2}\left[\partial_\mu(c_\beta H_3 - s_\beta G^0) - \frac{1}{2}(g_Y B_\mu - g_2 W_\mu^0)vs_\beta\right]^2$$

$$+ \frac{1}{2}\left[\partial_\mu(s_\beta H_3 + c_\beta G^0) + \frac{1}{2}(g_Y B_\mu - g_2 W_\mu^0)vc_\beta\right]^2 + ...$$

$$\supset \frac{1}{2}(\partial_\mu C_I - m_h\tilde{X}_\mu)^2 + \frac{1}{2}\left[\partial_\mu G^0 - \frac{ev}{s_{2W}}(c_W W_\mu^0 - s_W B_\mu)\right]^2 + ...$$

$$(D.1)$$

Clearly the masses of the neutral Higgs (both visible and hidden) are unaffected by the mixing, but the pseudoscalar will be. Using (C.2) and

$$c_W W_\mu^0 - s_W B_\mu = (c_\phi - s_W t_\epsilon s_\phi)Z_\mu + (s_\phi + s_W t_\epsilon c_\phi)\gamma_\mu'$$

$$(D.2)$$

we obtain

$$\mathcal{L} \supset -m_h\partial_\mu C_I \frac{1}{c_\epsilon}(-s_\phi Z_\mu + c_\phi \gamma_\mu') - M_{Z^0}\partial_\mu G^0((c_\phi - s_W t_\epsilon s_\phi)Z_\mu + (s_\phi + s_W t_\epsilon c_\phi)\gamma_\mu')$$

$$\supset -Z_\mu\left(-m_h\frac{s_\phi}{c_\epsilon}\partial_\mu C_I + M_{Z^0}(c_\phi - s_W t_\epsilon s_\phi)\partial_\mu G^0\right) - \gamma_\mu'\left(m_h\frac{c_\phi}{c_\epsilon}\partial_\mu C_I + M_{Z^0}(s_\phi + s_W t_\epsilon c_\phi)\partial_\mu G^0\right)$$

$$(D.3)$$

Thus

$$
\begin{aligned}
m_+ G_Z =& M_{Z^0}(c_\phi - s_W t_\epsilon s_\phi)G^0 - m_h \frac{s_\phi}{c_\epsilon}C_I \\
m_- G_{\gamma'} =& M_{Z^0}(s_\phi + s_W t_\epsilon c_\phi)G^0 + m_h \frac{c_\phi}{c_\epsilon}C_I
\end{aligned}
\tag{D.4}
$$

and

$$
\begin{aligned}
G^0 =& \frac{c_\epsilon}{M_{Z^0} m_h}\left[\frac{m_h c_\phi m_+}{c_\epsilon}G_Z + \frac{m_h s_\phi m_-}{c_\epsilon}G_{\gamma'}\right] \\
=& \frac{1}{M_{Z^0}}\left[c_\phi m_+ G_Z + s_\phi m_- G_{\gamma'}\right] \\
C_I =& \frac{c_\epsilon}{m_h}\left[-(s_\phi + s_W t_\epsilon c_\phi)m_+ G_Z + (c_\phi - s_W t_\epsilon s_\phi)m_- G_{\gamma'}\right].
\end{aligned}
\tag{D.5}
$$

We can also write this as

$$
\begin{aligned}
G^0 =& \cos\psi\, G_Z + \sin\psi\, G_{\gamma'} \\
C_I =& -\sin\psi\, G_Z + \cos\psi\, G_{\gamma'} \\
\tan\psi =& (\tan\phi)\frac{m_-}{m_+} = \frac{(s_\phi + s_W t_\epsilon c_\phi)m_+}{(c_\phi - s_W t_\epsilon s_\phi)m_-}.
\end{aligned}
\tag{D.6}
$$

E   Higgs portal mixing

With the Lagrangian density

$$
\mathcal{L} \supset \int d^2\theta\left(\frac{1}{4}B^\alpha B_\alpha + \frac{1}{4}X^\alpha X_\alpha - \frac{\chi}{2}B^\alpha X_\alpha\right) + c.c.,
\tag{E.1}
$$

we need the D-term mixing; we write $\hat{D}_Y \equiv -g_Y \sum_\phi \phi^\dagger \hat{Y}\phi, \hat{D}_X \equiv -g_h \sum_\phi \phi^\dagger \hat{Q}_X \phi$ as the D-terms in the absence of mixing, then we have

$$
\mathcal{L} \supset \frac{1}{2}D_Y^2 + \frac{1}{2}D_X^2 - \chi D_Y D_X - D_Y \hat{D}_Y - D_X \hat{D}_X
\tag{E.2}
$$

which leads to

$$
\begin{aligned}
D_X =& \frac{1}{1-\chi^2}(\hat{D}_X + \chi\hat{D}_Y) \\
D_Y =& \frac{1}{1-\chi^2}(\hat{D}_Y + \chi\hat{D}_X)
\end{aligned}
\tag{E.3}
$$

and thus

$$
\begin{aligned}
V \to& \frac{1}{2}\frac{1}{1-\chi^2}\left[\hat{D}_X^2 + \hat{D}_Y^2 + 2\chi\hat{D}_X\hat{D}_Y\right], \\
V_{\text{Portal}} \equiv& \frac{\chi}{1-\chi^2}\hat{D}_X\hat{D}_Y.
\end{aligned}
\tag{E.4}
$$

25

The relevant part of the potential for us involves the Higgses; we can write the portal term as

$$V_{\text{Portal}} = \frac{\chi}{1-\chi^2} g_Y g_h (|H_+|^2 - |H_-|^2)(\frac{1}{2}|H_u|^2 - \frac{1}{2}|H_d|^2) \tag{E.5}$$

$$= \frac{\chi g_Y g_h}{1-\chi^2} (|H_+|^2 - |H_-|^2)\left[\frac{1}{2}|H_u^+|^2 + \frac{1}{2}\left(\frac{1}{\sqrt{2}}v\sin\beta + H_u^0\right)^2 - \frac{1}{2}|H_d^-|^2 - \frac{1}{2}\left(\frac{1}{\sqrt{2}}v\cos\beta + H_d^0\right)^2\right].$$

Immediately we can extract the effective Fayet-Iliopoulos term:

$$V_{FI} = \frac{g_h^2}{2}(|H_+|^2 - |H_-|^2 - \xi)^2$$

$$= \frac{1}{2}(\hat{D}_h + \xi/g_h)^2$$

$$\xi \approx (\chi/g_h)\langle \hat{D}_Y \rangle$$

$$= (\chi/g_h)g_Y \frac{v^2}{4}\cos 2\beta. \tag{E.6}$$

However, we can also extract the Higgs mass mixing. Writing

$$H_+ = \frac{v_+}{\sqrt{2}} + \frac{1}{\sqrt{2}}(x_R + ix_I)$$

$$H_u^0 = \frac{1}{\sqrt{2}}[s_\beta v + h_u^0 + i(c_\beta A - s_\beta G^0)]$$

$$H_d^0 = \frac{1}{\sqrt{2}}[c_\beta v + h_d^0 + i(s_\beta A + c_\beta G^0)]$$

$$\begin{pmatrix} h_d^0 \\ h_u^0 \end{pmatrix} = \begin{pmatrix} \cos\alpha & -\sin\alpha \\ \sin\alpha & \cos\alpha \end{pmatrix} \begin{pmatrix} H \\ h \end{pmatrix} \tag{E.7}$$

and using the standard shorthand $c_\beta \equiv \cos\beta, c_\alpha \equiv \cos\alpha, c_{\alpha+\beta} \equiv \cos(\alpha+\beta)$ etc, we have

$$V \supset -\frac{t_\epsilon}{c_\epsilon} g_Y g_h |\frac{v_+}{\sqrt{2}} + \frac{1}{\sqrt{2}}(x_R + ix_I)|^2$$

$$\times \left[\frac{1}{2}|\frac{1}{\sqrt{2}}[s_\beta v + h_u^0 + i(c_\beta A - s_\beta G^0)]|^2 - \frac{1}{2}|\frac{1}{\sqrt{2}}[c_\beta v + h_d^0 + i(s_\beta A + c_\beta G^0)]|^2\right]$$

$$\supset -\frac{t_\epsilon}{c_\epsilon} g_Y g_h \frac{1}{2} v_+ v x_R \left[s_{\alpha+\beta}h - c_{\alpha+\beta}H\right]$$

$$\equiv \frac{1}{2}M_m^2 x_R \left[-s_{\alpha+\beta}h + c_{\alpha+\beta}H\right]$$

$$M_m^2 \equiv \frac{t_\epsilon}{c_\epsilon} g_Y g_h v \frac{\sqrt{2}\Delta}{\lambda_S}$$

$$= \frac{t_\epsilon}{c_\epsilon} 2M_Z s_W m_{\gamma'} \approx -2\chi s_W M_Z m_{\gamma'}. \tag{E.8}$$

So then we must redefine our Higgses: the mass mixing matrix in the basis (x_+, h, H) is

$$\mathcal{M}_{\text{Higgs}}^2 = \begin{pmatrix} m_+^2 & -s_{\alpha+\beta}M_m^2 & c_{\alpha+\beta}M_m^2 \\ -s_{\alpha+\beta}M_m^2 & m_h^2 & 0 \\ c_{\alpha+\beta}M_m^2 & 0 & m_H^2 \end{pmatrix}. \tag{E.9}$$

26

To first order in $M_m^2/m_{h,H}^2$ this is diagonalised via

$$
\begin{pmatrix} x_+ \\ h \\ H \end{pmatrix} = \begin{pmatrix} 1 & -\frac{s_{\alpha+\beta}M_m^2}{m_h^2-m_+^2} & \frac{c_{\alpha+\beta}M_m^2}{m_H^2-m_+^2} \\ \frac{s_{\alpha+\beta}M_m^2}{m_h^2-m_+^2} & 1 & 0 \\ -\frac{c_{\alpha+\beta}M_m^2}{m_H^2-m_+^2} & 0 & 1 \end{pmatrix} \begin{pmatrix} x'_R \\ h' \\ H' \end{pmatrix}. \tag{E.10}
$$

Since we often find $m_H^2 \gg m_h^2$ however the above will usually reduce to mixing between the hidden and lightest Higgs. In this case we can approximate

$$
\begin{pmatrix} x_R \\ h \end{pmatrix} \approx \begin{pmatrix} 1 & u \\ -u & 1 \end{pmatrix} \begin{pmatrix} x'_R \\ h' \end{pmatrix}
$$

$$
u \approx \frac{-s_{\alpha+\beta}M_m^2}{m_h^2-m_+^2} \approx s_{\alpha+\beta}2\chi s_W \frac{M_Z m_{\gamma'}}{m_h^2}. \tag{E.11}
$$

Thus very roughly $u \sim \chi s_W m_{\gamma'}/m_h$ for large $\tan\beta$.

E.1 Spin-independent nucleon cross-sections

Here we would like to estimate the cross-sections for our Majorana hidden fermion $\tilde{O}_1 = \begin{pmatrix} \tilde{o}_1 \\ \bar{\tilde{o}}_1 \end{pmatrix}$ on nucleons that take place via the Higgs portal term. The Higgs portal leads to an effective four-point interaction

$$
\mathcal{L} \supset f_N \left(\overline{\tilde{O}}_1 \tilde{O}_1 \overline{N}N \right) \tag{E.12}
$$

and we can consider different f_p, f_n for protons and neutrons respectively. Consider that the dark matter particle is a Majorana combination of $\tilde{\lambda}$ and $\tilde{h}_+$ fermions, $\tilde{o}_1 \approx \cos\theta_1 \tilde{h}_+ + \sin\theta_1 \tilde{\lambda}$. The coupling to the Hidden higgs is via the kinetic vertex

$$
\mathcal{L} \supset -\sqrt{2}g_h H_+^*(\tilde{h}_+\tilde{\lambda}) + c.c.
$$
$$
\supset -g_h \cos\theta_1 \sin\theta_1 x_R[(\tilde{o}_1\tilde{o}_1) + (\bar{\tilde{o}}_1\bar{\tilde{o}}_1)]
$$
$$
\supset -g_h \cos\theta_1 \sin\theta_1 x_R \overline{\tilde{O}}_1 \tilde{O}_1 \tag{E.13}
$$

where now $\tilde{O}_1$ is in Dirac form, $\tilde{O}_1 = \begin{pmatrix} \tilde{o}_1 \\ \bar{\tilde{o}}_1 \end{pmatrix}$. Now let us write the coupling of the MSSM Higgs to nucleons as $-a_N h\overline{N}N$.

$$
\mathcal{L} \supset -g_h \cos\theta_1 \sin\theta_1 [x'_R + uh']\overline{\tilde{O}}_1 \tilde{O}_1 - a_N[-ux'_R + h']\overline{N}N - \frac{1}{2}m_1^2(x'_R)^2 - \frac{1}{2}m_2^2(h')^2
$$
$$
\to u a_N \cos\theta_1 \sin\theta_1 \left[\frac{1}{m_1^2} - \frac{1}{m_2^2}\right] \left(\overline{\tilde{O}}_1 \tilde{O}_1 \overline{N}N \right)
$$
$$
\approx a_N \cos\theta_1 \sin\theta_1 s_{\alpha+\beta}2\chi s_W \frac{M_Z m_{\gamma'}}{m_+^2 m_h^2} \left(\overline{\tilde{O}}_1 \tilde{O}_1 \overline{N}N \right)
$$
$$
\to f_N \approx a_N \sin 2\theta_1 s_{\alpha+\beta}\chi s_W \frac{M_Z m_{\gamma'}}{m_+^2 m_h^2}. \tag{E.14}
$$

So then our direct detection amplitude should be approximately given by the coefficient above.

The coupling of the MSSM Higgs to nucleons is determined by its coupling to quarks. These come from

$$
\begin{aligned}
\mathcal{L} &\supset -Y_U H_U qu - Y_D H_D qd \\
&\supset -\frac{c_\alpha}{v s_\beta} h(m_U \bar{u} u) - \frac{s_\alpha}{v c_\beta} h(m_D \bar{d} d).
\end{aligned}
\tag{E.15}
$$

Then we use that [78]

$$
\begin{aligned}
\langle N | m_q \bar{q} q | N \rangle &= m_n f_{Tq}^{(N)} \\
\langle N | m_Q \overline{Q} Q | N \rangle_{Q=c,b,t} &= \frac{2}{27} m_N \left[1 - \sum_{q=u,d,s} f_{Tq}^{(N)} \right] \\
&\equiv \frac{2}{27} m_N \left[1 - \tilde{F}^{(N)} \right]
\end{aligned}
\tag{E.16}
$$

to give

$$
a_N = \frac{c_\alpha}{v s_\beta} m_N \left[\frac{4}{27}(1 - \tilde{F}) + f_{Tu}^{(N)} \right] + \frac{s_\alpha}{v c_\beta} m_N \left[\frac{2}{27}(1 - \tilde{F}) + f_{Td}^{(N)} + f_{Ts}^{(N)} \right].
\tag{E.17}
$$

If we consider large $\tan\beta$ with $\beta = \pi/2 - \delta$, $\alpha \approx -\delta$ we have $s_\alpha \approx -\delta, c_\alpha \approx 1, c_\beta \approx \delta, s_\beta \approx 1$ and so $a_N \approx \frac{m_N}{v} \left[\frac{2}{27}(1 - \tilde{F}) + f_{Tu}^{(N)} - f_{Td}^{(N)} - f_{Ts}^{(N)} \right]$. Let us then simply define

$$
a_N \equiv \frac{m_N}{v} \hat{f}^{(N)}.
\tag{E.18}
$$

There are large uncertainties in the value of $\hat{f}^{(N)}$, however it is approximately equal for protons and neutrons, and varies from about 0.03 to 0.44. We can then take an approximate value for the amplitude for a Majorana fermion scattering on nucleons to be

$$
f_N \approx \sin 2\theta_1 s_{\alpha+\beta} \chi s_W \frac{M_Z m_{\gamma'}}{m_+^2 m_h^2} \frac{m_N}{v} \hat{f}^{(N)}.
\tag{E.19}
$$

Taking the large $\tan\beta$ values, $m_h = 115$ GeV and $\hat{f}^{(N)} \sim 0.1$ we obtain

$$
f_N \approx 3 \times 10^{-9} (\text{GeV})^{-2} \times \left(\sin 2\theta_1 \right) \left(\frac{\chi s_W}{0.001} \right) \left(\frac{\text{GeV}}{m_{\gamma'}} \right)
\tag{E.20}
$$

This is clearly a very small effect. This translates into a cross-section for scattering on a single nucleon of

$$
\begin{aligned}
\sigma_N^{\text{SI, Portal}} &= \frac{4 m_{\tilde{o}1}^2 m_N^2}{\pi (m_N + m_{\tilde{o}1})^2} f_N^2 \\
&\approx 2 \times 10^{-45} \text{cm}^2 \times \left(\frac{m_{\tilde{o}1}^2}{(m_N + m_{\tilde{o}1})^2} \right) \left(\sin 2\theta_1 \right)^2 \left(\frac{\chi s_W}{0.001} \right)^2 \left(\frac{\text{GeV}}{m_{\gamma'}} \right)^2.
\end{aligned}
\tag{E.21}
$$

This corresponds well to the values that we find in the plots.

The above will be supplemented by contributions from s-channel squark exchange. Very roughly for these we have effective four-point interactions of the Majorana fermion with quarks with coupling $f_q \sim \frac{g^2}{M_{\tilde{Q}}^2} |U_{\tilde{b}\tilde{o}_1}|^2$, where $\tilde{b} = \sum_n U_{b\tilde{o}_n} \tilde{o}_n$ is the Bino, which mixes most strongly with the lightest hidden state. By considering the mass mixing matrix in section B.2 we can conclude that (in the absence of direct mass mixing) the mixing is simply $\sim \chi M_\lambda$, so we have $U_{\tilde{b}\tilde{o}_1} \sim \chi$, and thus

$$f_N \sim \frac{g_Y^2}{M_{\tilde{Q}}^2} \chi^2 \sum_q \frac{m_N}{m_q} f_{Tq}^N \tag{E.22}$$

and thus

$$\sigma_N^{\text{SD, Squark}} \sim 10^{-48} \text{cm}^2 \times \left(\frac{m_{\tilde{o}_1}^2}{(m_N + m_{\tilde{o}_1})^2} \right) \left(\frac{s_W \chi}{0.001} \right)^4 \left(\frac{100 \text{GeV}}{M_{\tilde{Q}}} \right)^4. \tag{E.23}$$

References

[1] M. Pospelov, A. Ritz and M. B. Voloshin, *Secluded WIMP Dark Matter*, Phys. Lett. **B662** (2008) 53–61 [0711.4866].

[2] N. Arkani-Hamed, D. P. Finkbeiner, T. R. Slatyer and N. Weiner, *A Theory of Dark Matter*, Phys. Rev. **D79** (2009) 015014 [0810.0713].

[3] M. Pospelov and A. Ritz, *Astrophysical Signatures of Secluded Dark Matter*, Phys. Lett. **B671** (2009) 391–397 [0810.1502].

[4] N. Arkani-Hamed and N. Weiner, *LHC Signals for a SuperUnified Theory of Dark Matter*, JHEP **12** (2008) 104 [0810.0714].

[5] **PAMELA Collaboration** Collaboration, O. Adriani *et. al.*, *An anomalous positron abundance in cosmic rays with energies 1.5-100 GeV*, Nature **458** (2009) 607–609 [0810.4995].

[6] J. Chang, J. Adams, H. Ahn, G. Bashindzhagyan, M. Christl *et. al.*, *An excess of cosmic ray electrons at energies of 300-800 GeV*, Nature **456** (2008) 362–365.

[7] **The Fermi LAT Collaboration** Collaboration, A. A. Abdo *et. al.*, *Measurement of the Cosmic Ray e+ plus e- spectrum from 20 GeV to 1 TeV with the Fermi Large Area Telescope*, Phys.Rev.Lett. **102** (2009) 181101 [0905.0025].

[8] **DAMA** Collaboration, R. Bernabei *et. al.*, *First results from DAMA/LIBRA and the combined results with DAMA/NaI*, Eur. Phys. J. **C56** (2008) 333–355 [0804.2741].

[9] **CoGeNT collaboration** Collaboration, C. Aalseth *et. al.*, *Results from a Search for Light-Mass Dark Matter with a P-type Point Contact Germanium Detector*, Phys.Rev.Lett. **106** (2011) 131301 [1002.4703].

[10] C. Aalseth, P. Barbeau, J. Colaresi, J. Collar, J. Leon *et. al.*, *Search for an Annual Modulation in a P-type Point Contact Germanium Dark Matter Detector*, 1106.0650.

[11] G. Angloher, M. Bauer, I. Bavykina, A. Bento, C. Bucci *et. al.*, *Results from 730 kg days of the CRESST-II Dark Matter Search*, 1109.0702.

[12] J. Collar, *A Realistic Assessment of the Sensitivity of XENON10 and XENON100 to Light-Mass WIMPs*, 1106.0653.

[13] J. Collar, *A comparison between the low-energy spectra from CoGeNT and CDMS*, 1103.3481.

[14] **XENON100** Collaboration, E. Aprile *et. al.*, *Dark Matter Results from 100 Live Days of XENON100 Data*, 1104.2549.

[15] **CDMS-II Collaboration** Collaboration, Z. Ahmed *et. al.*, *Results from a Low-Energy Analysis of the CDMS II Germanium Data*, *Phys.Rev.Lett.* **106** (2011) 131302 [1011.2482].

[16] E. J. Chun and J.-C. Park, *Dark matter and sub-GeV hidden U(1) in GMSB models*, *JCAP* **0902** (2009) 026 [0812.0308].

[17] C. Cheung, J. T. Ruderman, L.-T. Wang and I. Yavin, *Kinetic Mixing as the Origin of Light Dark Scales*, *Phys. Rev.* **D80** (2009) 035008 [0902.3246].

[18] A. Katz and R. Sundrum, *Breaking the Dark Force*, *JHEP* **06** (2009) 003 [0902.3271].

[19] D. E. Morrissey, D. Poland and K. M. Zurek, *Abelian Hidden Sectors at a GeV*, *JHEP* **07** (2009) 050 [0904.2567].

[20] T. Cohen, D. J. Phalen, A. Pierce and K. M. Zurek, *Asymmetric Dark Matter from a GeV Hidden Sector*, *Phys. Rev.* **D82** (2010) 056001 [1005.1655].

[21] S. A. Abel, M. D. Goodsell, J. Jaeckel, V. V. Khoze and A. Ringwald, *Kinetic Mixing of the Photon with Hidden U(1)s in String Phenomenology*, *JHEP* **07** (2008) 124 [0803.1449].

[22] M. Goodsell, *Light Hidden U(1)s from String Theory*, 0912.4206.

[23] M. Goodsell, J. Jaeckel, J. Redondo and A. Ringwald, *Naturally Light Hidden Photons in LARGE Volume String Compactifications*, *JHEP* **11** (2009) 027 [0909.0515].

[24] M. Goodsell and A. Ringwald, *Light hidden-sector U(1)s in string compactifications*, *Fortsch.Phys.* **58** (2010) 716–720 [1002.1840].

[25] J. J. Heckman and C. Vafa, *An Exceptional Sector for F-theory GUTs*, *Phys.Rev.* **D83** (2011) 026006 [1006.5459].

[26] M. Bullimore, J. P. Conlon and L. T. Witkowski, *Kinetic mixing of U(1)s for local string models*, *JHEP* **11** (2010) 142 [1009.2380].

[27] M. Cicoli, M. Goodsell, J. Jaeckel and A. Ringwald, *Testing String Vacua in the Lab: From a Hidden CMB to Dark Forces in Flux Compactifications*, *JHEP* **1107** (2011) 114 [1103.3705].

[28] M. Williams, C. P. Burgess, A. Maharana and F. Quevedo, *New Constraints (and Motivations) for Abelian Gauge Bosons in the MeV-TeV Mass Range*, 1103.4556.

[29] J. J. Heckman and S.-J. Rey, *Baryon and Dark Matter Genesis from Strongly Coupled Strings*, *JHEP* **1106** (2011) 120 [1102.5346].

[30] K. R. Dienes, C. F. Kolda and J. March-Russell, *Kinetic mixing and the supersymmetric gauge hierarchy*, *Nucl. Phys.* **B492** (1997) 104–118 [hep-ph/9610479].

[31] A. Lukas and K. S. Stelle, *Heterotic anomaly cancellation in five dimensions*, *JHEP* **01** (2000) 010 [hep-th/9911156].

[32] R. Blumenhagen, G. Honecker and T. Weigand, *Loop-corrected compactifications of the heterotic string with line bundles*, *JHEP* **06** (2005) 020 [hep-th/0504232].

[33] S. A. Abel and B. W. Schofield, *Brane-antibrane kinetic mixing, millicharged particles and SUSY breaking*, *Nucl. Phys.* **B685** (2004) 150–170 [hep-th/0311051].

[34] D. Lust and S. Stieberger, *Gauge threshold corrections in intersecting brane world models*, *Fortsch. Phys.* **55** (2007) 427–465 [hep-th/0302221].

[35] S. A. Abel, J. Jaeckel, V. V. Khoze and A. Ringwald, *Illuminating the hidden sector of string theory by shining light through a magnetic field*, *Phys. Lett.* **B666** (2008) 66–70 [hep-ph/0608248].

[36] K. Benakli and M. D. Goodsell, *Dirac Gauginos and Kinetic Mixing, Nucl. Phys.* **B830** (2010) 315–329 [0909.0017].

[37] F. Gmeiner and G. Honecker, *Complete Gauge Threshold Corrections for Intersecting Fractional D6-Branes: The Z6 and Z6' Standard Models, Nucl.Phys.* **B829** (2010) 225–297 [0910.0843].

[38] C. Burgess, J. Conlon, L.-Y. Hung, C. Kom, A. Maharana *et. al., Continuous Global Symmetries and Hyperweak Interactions in String Compactifications, JHEP* **0807** (2008) 073 [0805.4037].

[39] A. Hook, E. Izaguirre and J. G. Wacker, *Model Independent Bounds on Kinetic Mixing*, 1006.0973.

[40] D. Feldman, Z. Liu and P. Nath, *The Stueckelberg Z' extension with kinetic mixing and milli-charged dark matter from the hidden sector, Phys. Rev.* **D75** (2007) 115001 [hep-ph/0702123].

[41] E. Dudas, Y. Mambrini, S. Pokorski and A. Romagnoni, *(In)visible Z-prime and dark matter, JHEP* **0908** (2009) 014 [0904.1745].

[42] Y. Mambrini, *A Clear Dark Matter gamma ray line generated by the Green-Schwarz mechanism, JCAP* **0912** (2009) 005 [0907.2918].

[43] Y. Mambrini, *Specific Dark Matter signatures from hidden U(1), PoS* **QFTHEP2010** (2010) 027 [1012.0447].

[44] Y. Mambrini, *The kinetic dark-mixing in the light of CoGENT and XENON100, JCAP* **1009** (2010) 022 [1006.3318].

[45] Y. Mambrini, *The ZZ' kinetic mixing in the light of the recent direct and indirect dark matter searches, JCAP* **1107** (2011) 009 [1104.4799].

[46] G. Belanger, F. Boudjema, A. Pukhov and A. Semenov, *MicrOMEGAs: A Program for calculating the relic density in the MSSM, Comput.Phys.Commun.* **149** (2002) 103–120 [hep-ph/0112278].

[47] G. Belanger, F. Boudjema, A. Pukhov and A. Semenov, *MicrOMEGAs 2.0: A Program to calculate the relic density of dark matter in a generic model, Comput.Phys.Commun.* **176** (2007) 367–382 [hep-ph/0607059].

[48] G. Belanger, F. Boudjema, A. Pukhov and A. Semenov, *micrOMEGAs 2.0.7: A program to calculate the relic density of dark matter in a generic model, Comput.Phys.Commun.* **177** (2007) 894–895.

[49] G. Belanger, F. Boudjema, A. Pukhov and A. Semenov, *Dark matter direct detection rate in a generic model with micrOMEGAs 2.2, Comput.Phys.Commun.* **180** (2009) 747–767 [0803.2360].

[50] G. Belanger, F. Boudjema, A. Pukhov and A. Semenov, *micrOMEGAs: A Tool for dark matter studies*, 1005.4133.

[51] M. Pospelov, *Secluded U(1) below the weak scale, Phys. Rev. D* **80** (Nov, 2009) 095002 [0811.1030].

[52] R. Essig, P. Schuster and N. Toro, *Probing Dark Forces and Light Hidden Sectors at Low-Energy e+e- Colliders, Phys. Rev.* **D80** (2009) 015003 [0903.3941].

[53] J. D. Bjorken, R. Essig, P. Schuster and N. Toro, *New Fixed-Target Experiments to Search for Dark Gauge Forces, Phys. Rev.* **D80** (2009) 075018 [0906.0580].

[54] J. Blumlein and J. Brunner, *New Exclusion Limits for Dark Gauge Forces from Beam-Dump Data, Phys. Lett.* **B701** (2011) 155–159 [1104.2747].

[55] **A1** Collaboration, H. Merkel *et. al., Search for light gauge bosons of the dark sector at MAMI*, 1101.4091.

[56] R. Essig, P. Schuster, N. Toro and B. Wojtsekhowski, *An Electron Fixed Target Experiment to Search for a New Vector Boson A' Decaying to e+e-, JHEP* **02** (2011) 009 [1001.2557].

[57] S. Abrahamyan *et. al., Search for a new gauge boson in the A' Experiment (APEX)*, 1108.2750.

[58] M. Freytsis, G. Ovanesyan and J. Thaler, *Dark Force Detection in Low Energy e-p Collisions*, *JHEP* **01** (2010) 111 [0909.2862].

[59] S. Andreas and A. Ringwald, *Status of sub-GeV Hidden Particle Searches*, *PATRAS Proceedings* (2010) [1008.4519].

[60] **WMAP** Collaboration, E. Komatsu *et. al.*, *Seven-Year Wilkinson Microwave Anisotropy Probe (WMAP) Observations: Cosmological Interpretation*, *Astrophys. J. Suppl.* **192** (2011) 18 [1001.4538].

[61] F. Giuliani, *Are direct search experiments sensitive to all spin-independent WIMP candidates?*, *Phys.Rev.Lett.* **95** (2005) 101301 [hep-ph/0504157].

[62] J. L. Feng, J. Kumar, D. Marfatia and D. Sanford, *Isospin-Violating Dark Matter*, *Phys. Lett.* **B703** (2011) 124–127 [1102.4331].

[63] M. T. Frandsen *et. al.*, *On the DAMA and CoGeNT Modulations*, 1105.3734.

[64] C. McCabe, *DAMA and CoGeNT without astrophysical uncertainties*, 1107.0741.

[65] M. T. Frandsen, F. Kahlhoefer, S. Sarkar and K. Schmidt-Hoberg, *Direct detection of dark matter in models with a light Z'*, 1107.2118.

[66] C. Arina, J. Hamann and Y. Y. Y. Wong, *A Bayesian view of the current status of dark matter direct searches*, 1105.5121.

[67] E. Behnke, J. Behnke, S. Brice, D. Broemmelsiek, J. Collar *et. al.*, *Improved Limits on Spin-Dependent WIMP-Proton Interactions from a Two Liter CF_3I Bubble Chamber*, *Phys.Rev.Lett.* **106** (2011) 021303 [1008.3518].

[68] **Super-Kamiokande** Collaboration, S. Desai *et. al.*, *Search for dark matter WIMPs using upward through-going muons in Super-Kamiokande*, *Phys. Rev.* **D70** (2004) 083523 [hep-ex/0404025]. arXiv:hep-ex/0404025v2.

[69] M. Felizardo *et. al.*, *Final Analysis and Results of the Phase II SIMPLE Dark Matter Search*, 1106.3014.

[70] J. Collar, *Comments on 'Final Analysis and Results of the Phase II SIMPLE Dark Matter Search'*, 1106.3559.

[71] T. S. Collaboration, *Reply to arxiv:1106.3559 by J.I. Collar*, 1107.1515.

[72] A. Semenov, *LanHEP: A Package for automatic generation of Feynman rules in gauge models*, hep-ph/9608488.

[73] A. Semenov, *LanHEP: A package for automatic generation of Feynman rules from the Lagrangian*, *Comput.Phys.Commun.* **115** (1998) 124–139.

[74] A. Semenov, *LanHEP: A Package for automatic generation of Feynman rules in field theory. Version 2.0*, hep-ph/0208011.

[75] A. Semenov, *LanHEP: A Package for the automatic generation of Feynman rules in field theory. Version 3.0*, *Comput.Phys.Commun.* **180** (2009) 431–454 [0805.0555].

[76] A. Semenov, *LanHEP - a package for automatic generation of Feynman rules from the Lagrangian. Updated version 3.1*, 1005.1909.

[77] B. Allanach, *SOFTSUSY: a program for calculating supersymmetric spectra*, *Comput.Phys.Commun.* **143** (2002) 305–331 [hep-ph/0104145].

[78] G. Jungman, M. Kamionkowski and K. Griest, *Supersymmetric dark matter*, *Phys.Rept.* **267** (1996) 195–373 [hep-ph/9506380].